


A STUDY OF THE EMBRITTLEMENT AND TOUGHENING OF FE - 40% CR ALLOYS

Elizabeth Anne DeMarsh

A dissertation submitted to the Faculty of Engineering, University of the Witwatersrand, Johannesburg, in fulfilment of the requirements for the degree of Master of Science in Engineering.

Johannesburg, 1986

I declare that this dissertation is my own, unaided work. It is being submitted for the degree of Master of Science in Engineering, in the University of the Witwatersrand, Johannesburg. It has not been submitted before for any degree or examination in any other University.


Signature

31st day of March, 1986.

ABSTRACT

A study was made of the mechanisms by which Fe - 40% Cr alloys are embrittled. This knowledge was used to develop processes by which the alloys could be rendered ductile below ambient temperatures. The interstitial levels were reduced through melting practice. The alloys were rolled from a temperature above the σ -phase formation range to below the recrystallization temperature and within the σ -phase formation range. This served the dual purpose of refining the grain size and allowing σ -phase to form at the grain boundaries and on existing precipitates. The effective result of the formation and dissolution of σ -phase in this bcc alloy was to increase the mobile dislocation density, decrease the temperature sensitivity of the yield stress and thereby reduce the DBTT to below ambient temperatures.

Proper stabilization, the addition of aluminium as a deoxidizer and the addition of nickel which distorts the lattice and therefore entraps the interstitials were all found to be advantageous to the toughness and ductility.

In memory of my mother

Noreen Elizabeth Dotey

and to

Nicole Elizabeth DeMarsh

who inspired me to finish this work.

ACKNOWLEDGEMENTS

The assistance of many individuals was greatly appreciated throughout the execution of this work, which was carried out while employed by The Council for Mineral Technology.

Thanks to Dr P.T. Wedepohl and the staff of the Physical Metallurgy Division with special thanks to John Maskrey, Chris Millward and Chris Fletcher.

The assistance of Mr E.A. Viljoen and Mrs J. Russell for the micro-probe analysis, Dr E.J. Oosthuizen and Mrs J. Mostert for the image analysis, and Mr P. Ellis on the SEM are all greatly appreciated.

For the use of the transmission electron microscope and for their helpful time, thanks go to the people at ISCOR.

This work was carried out with the continuing interest of Professor G. Garrett, Dr J. Bee and Dr P. Wedepohl. I thank them for their time and interest.

Finally, I want to thank Grant, my husband, for his constant support.

CONTENTSPage

DECLARATION	ii
ABSTRACT	iii
DEDICATION	iv
ACKNOWLEDGEMENTS	v
CONTENTS	vi
LIST OF FIGURES	viii
LIST OF TABLES	xi
1. INTRODUCTION AND BACKGROUND	1
2. LITERATURE REVIEW	3
2.1 Introduction	3
2.2 Fracture of Ferritic Stainless Steels	3
2.3 Interstitials - Content and Form	14
2.4 Stabilization	15
2.5 High Temperature Embrittlement	18
2.6 475 °C Embrittlement	19
2.7 Sigma-Phase Embrittlement	22
2.8 Rhenium Ductilizing Effect	23
2.9 Summary	25
3. EXPERIMENTAL PROCEDURE	26
3.1 Melting Practice	26
3.2 Fabrication	27
3.3 Heat Treatment and Specimen Preparation	29
3.4 Mechanical Testing	30
3.5 Metallography	30
3.6 Fractography	32
3.7 Alloyed Fe - 40% Cr	32
4. RESULTS	35
4.1 Metallography	35
4.2 Mechanical Tests	42
4.3 Deformation and Fracture Mechanisms	55
4.3.1 Slow-bend and Charpy V-notch specimens	55
4.3.2 Tensile test samples	62
4.4 Alloyed Fe - 40% Cr	63

	<u>Page</u>
5. DISCUSSION	66
5.1 Introduction	66
5.2 Rolling Parameters	66
5.3 Sigma-Phase Embrittled Material	69
5.4 "Tough" material	73
5.5 High temperature Embrittled Material	81
5.6 Alloyed Fe - 40% Cr	85
6. SUMMARY	91
7. CONCLUSIONS AND RECOMMENDATIONS FOR FURTHER WORK	93
7.1 Conclusion	93
7.2 Recommendations for Further Work	93
8. REFERENCES	95

LIST OF FIGURES

Page

- 2.1 Characteristic width of an edge dislocation which affects the Peierls-Nabarro stress. 4
- 2.2 (a) Three stages associated with the development of an unstable cleavage fracture in a polycrystalline metal. 8
(b) Conditions under which non-propagating microcracks are not formed (1) and are formed (2) in a polycrystalline metal.¹⁴
- 2.3 Effect of test temperature on the critical resolved shear stress τ_y for slip and twinning in a typical BCC metal. Yielding occurs by twinning when $T < T_t$ and by slip at $T > T_t$.¹⁴ 9
- 2.4 Effect of sample thickness and cooling rate from an 1121 °C, 30 min. anneal, on the Fracture Appearance Transition Temperature (FATT).¹⁹ 12
- 2.5 Schematic showing how the crack tip field may be unable to capture dislocations and cause them to multiply when the dislocation density is low, but may do so when the dislocation density is higher.²¹ 13
- 2.6 The variation of the ductile-brittle transition temperature with dislocation density.²¹ 13
- 2.7 Solubility of carbon and nitrogen in 26% chromium steel versus temperature.²² 15
- 2.8 Phase diagram of the ... system according to Williams.³⁶ 20
- 2.9. Effects of solute content on ductile-to-brittle bend transition temperature of chromium alloys annealed at indicated temperatures.⁴⁹ 24

	<u>Page</u>
4.1 σ -phase nucleated on grain boundaries and precipitates.	36
4.2 Volume percent of precipitates as a function of heat treatment temperature.	40
4.3 Yield strength as a function of heat treatment temperature.	41
4.4 Impact energy versus heat treatment temperature.	44
4.5 Hardness versus heat treatment temperature.	45
4.6 Slow-bend DBTT curves for Fe - 40% Cr.	48
4.7 DBTT analysis; Sample 8 (1050 °C).	54
4.8 Fracture surface of a slow-bend specimen from Sample 1 (heat-treated at 700 °C) tested at ambient temperatures.	57
4.9 Fracture surface of a slow-bend specimen (Sample 8) showing sharp transition from ductile to brittle fracture.	58
4.10 Fracture surface of Sample 8 tested in slow-bend near the DBTT (-40 °C) showing a "mixed" fracture.	59
4.11 Deformation surface of slow-bend Sample 8 tested at -45 °C, immediately adjacent to the fracture surface.	60
4.12 Deformation surface of slow-bend Sample 8 tested at -45 °C, several grains from the fracture surface. (adjacent to the area of Figure 4.11).	61
5.1 SEM photomicrograph showing cracking of σ -phase during rolling from 750 to 600 °C.	68

	<u>Page</u>
5.2 SEM photomicrograph of a slow-bend deformation surface for σ -embrittled Sample 1 (700 °C).	70
5.3 Fracture surface of a σ -embrittled specimen (Sample 1) showing grain boundary decohesion, and a twin intercepting a grain boundary.	71
5.4 TEM photomicrograph of Sample 1 (heat-treated at 700 °C) showing recovery of dislocations.	73
5.5 Fracture surface of Sample 8 fractured above the DBTT (10 °C). Areas of cleavage are associated with large precipitates within the ductile fracture.	75
5.6 TEM photomicrograph of Sample 8 (1050 °C). A high dislocation density is present at the grain boundaries and precipitates.	77
5.7 S ₁ bands encountering grain boundaries of Sample 8 (1600 °C).	78
5.8 Deformation surface of Sample 8 fractured in slow-bend below the DBTT (-45 °C). Microcracking is occurring at the tips of twins.	79
5.9 TEM photomicrograph of a sample quenched from 1300 °C. Small precipitates, dislocation pinning and dislocation loops can be seen within the grains.	83

LIST OF TABLES

	<u>Page</u>
2.1 Effective postwelding brittleness preventers for high-chromium ferritic alloys. ³⁰	17
2.2 Effects of composition on 475 °C embrittlement in chromium-iron alloys. ³⁵	21
3.1 Composition of electrolytic Fe and Cr as reported by the manufacturers. (All maximum values) (wt.%).	26
3.2 The composition of the preliminary experimental melts.	28
3.3 Heat treatment temperatures.	29
3.4 Composition of alloyed Fe - 40% Cr.	33
4.1 ASTM grain sizes and average grain diameters for heat-treated samples.	37
4.2 Microprobe analysis of a random selection of precipitates in Fe - 40% Cr heat-treated at 700 and 1050 °C.	38
4.3 Ambient temperature Charpy impact energies (half size specimens).	42
4.4 Ambient temperature tensile test results.	43
4.5 Vickers hardness numbers.	43
4.6 DBTT values as determined from slow-bend curves.	45
4.7 Observed deformation and fracture mechanisms of slow-bend and Charpy impact specimens following different heat-treatments.	64

	<u>Page</u>
4.8 DBTT's and upper shelf energies for alloyed Fe - 40% Cr determined from Charpy impact tests.	64
4.9 Results of hardness tests and ambient temperature tensile tests for alloyed Fe - 40% Cr.	65
5.1 The Stabilizer: (C + N) ratios added and recovered for Alloys B and C.	86

1. INTRODUCTION AND BACKGROUND

To date, ferritic stainless steels have been used much less extensively in industry, as compared with austenitic grades of stainless steel. The limited use stems from an inherent limited ductility and/or toughness at ambient temperatures and poor weldability. However, they exhibit excellent corrosion and oxidation resistance and are relatively much less expensive than the nickel-containing austenitic stainless steels. They are also resistant to stress corrosion cracking, which is an inherent problem of the austenitic grades. These desirable properties of the ferritic stainless steels have resulted in an increased interest in an extension of their use.

The corrosion resistance of stainless steels is a function of the chromium content, thus leading to an interest in the higher chromium-containing ferritic grades. Although recent work has appeared to concentrate on a high chromium content range of 25 to 30 per cent,* Tomashov and Chernova^{1 2} found that even larger concentrations were beneficial. In a study of the corrosion resistance of iron-chromium alloys, they found that the passivation potential changed slowly in the favourable direction (negative) with increases in the chromium content above 40 per cent. However, the critical current density for passivation greatly increased for alloys with a chromium content greater than 40 per cent. Hence, it was suggested that the Fe-40%Cr alloy had the optimum passive characteristics.

The corrosion resistance for iron-chromium alloys containing 0.15 to 0.2 per cent palladium as a function of chromium content was also studied by Tomashov and Chernova¹. It was found that the minimum time for self-passivation, and the minimum amount of corrosion before passivation were again observed at a concentration around 40 per cent chromium.

The production and application of viable high chromium ferritic stainless steels will clearly depend on understanding the mechanisms

* All values are reported as weight percentages unless otherwise stated.

by which they are embrittled, and the development of processes by which they may be rendered ductile at, or below, ambient temperatures.

These alloys may be embrittled in several ways. These include the formation of various intermetallic phases, such as sigma (σ)-phase and the intermetallic compound formed during the phenomenon known as '475 °C embrittlement'. In addition, the interstitial content and the 'state' of those interstitials has been shown to be of vast importance to the ductility of these alloys. The works of Hochmann³ and of Binder and Spendelov⁴ first showed that ferritic chromium steels could be rendered ductile at ambient temperatures by reducing the carbon and nitrogen contents. They concluded that the reduction in toughness as the chromium content was increased above about 20 per cent, was not due to the chromium itself, as had been previously believed, but was related to other factors, especially the carbon and nitrogen contents of the steel.

In the present investigation, it was decided therefore to carry out a systematic study on the proposed optimum Fe - 40% Cr composition, with particular emphasis on the embrittling mechanisms and subsequent ductilization of these alloys.

2. LITERATURE REVIEW

2.1 Introduction

The aim of this literature review is to summarize the results of previous work concerning the fracture of ferritic stainless steels and body-centred cubic (bcc) metals, the effects of embrittling phases and interstitial solutes, and to consider the rhenium ductilizing effect in these alloys.

By understanding the kinetics of formation and dissolution of the intermetallic phases, they may be avoided during manufacture, or eliminated in the final product. The effects of interstitial

elements on the ductility of these alloys will also be presented. This will include their effects in solution, precipitated with iron and/or chromium, or combined in a more 'stable' form. The method by which these factors embrittle or ductilize ferritic stainless steels will be considered in terms of relevant theories of fracture.

The rhenium ductilizing effect is the observed phenomenon whereby the addition of iron (which is believed to be a "rhenium analcapse") to chromium, results in an improvement in ductility as compared to unalloyed chromium. The composition which has been proposed as being optimum for the iron-chromium system is very close to the composition of the alloys used in the present study.

It must be stressed that the majority of results within the literature survey relate to ferritic stainless steels with 20 to 30 per cent chromium, whereas the alloy studied was Fe - 40% Cr.

2.2 The Fracture of Ferritic Stainless Steels.

Metals of group VIB in the periodic table exhibit a particularly low solubility for interstitials, and a greater tendency for the interstitials to segregate at grain boundaries and dislocations, and this largely governs their low-temperature ductility. Body-centred cubic (bcc) metals have a higher Peierls-Nabarro stress and contain less mobile dislocations than face-centred cubic (fcc) metals⁶. In

the former, the yield stress is very sensitive to temperature and strain rate changes. This factor is directly related to the contribution to the yield stress of the temperature-sensitive Peierls-Nabarro stress⁶.

The Peierls-Nabarro or Peierls force is that force necessary to move a dislocation through a lattice. The Peierls force depends on (Figure 2.1):

1. the width of the dislocation, W , which is a measure of the distance over which the lattice is distorted due to the dislocation; and
2. the distance between similar planes (a).

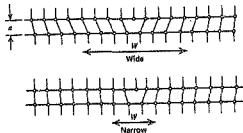


Figure 2.1 Characteristic width of an edge dislocation which affects the Peierls-Nabarro stress.⁷

The Peierls force decreases as a increases, therefore slip is preferred on closely packed planes.

W depends on the nature of the atomic bonding forces. In close-packed structures such as fcc and hcp, (hexagonal close-packed) the bonding forces are spherical in distribution and act along the line of centres between atoms. In these structures, W is large and the Peierls stress is small. However, when bonding forces are very directional, as for ionic and bcc crystals, W is small and the Peierls stress is large.

The Peierls stress depends on the short-range stress field of the dislocation. Therefore, it is sensitive to the thermal energy within the lattice, and thus to the test temperature. In close-packed crystals (fcc and hcp), the increase in the Peierls stress with decreasing temperature is insignificant, since the Peierls stress itself is negligible. As the temperature decreases, the thermal enhancement of dislocation motion is limited, therefore the Peierls stress increases. In bcc crystals, this increase in the Peierls stress does represent an increasing component of yield stress. Thus unlike fcc metals, bcc metals go through a transition from ductile to brittle fracture as the temperature is decreased or the strain rate is increased. The effect of the energy to fracture has been related in ferritic steels to a change in the microscopic fracture mechanism: transgranular cleavage at low temperatures and void coalescence at high temperatures⁶.

Gilbert et al⁸ studied the fracture of unalloyed chromium. They found that grain boundary ruptures were frequently the origin of brittle fracture in polycrystalline chromium and consequently single crystals were more ductile. They concluded that grain boundaries play an important role in crack initiation in bcc metals. It was also suggested that the reason for the brittleness of chromium was low crack propagation resistance, and this may be related to a lack of stress-relieving slip. This hypothesis was supported by Pollard⁹ who found no microcracks in Fe-26%Cr unloaded just before fracture and concluded therefore that crack nucleation rather than crack propagation is the important step in the brittle fracture of ferritic steels.

Hall¹⁰ and Petch¹¹ have shown that the variation of the lower

yield point of iron with grain size can be expressed by the equation:

$$\sigma_y = \sigma_i + k_y d^{-1/2} \quad \text{..... (2.1)}$$

where σ_y is the flow or yield stress;

k_y is the Hall-Petch slope;

σ_i is the lattice friction stress; and

d is the grain size.

With the aid of the Hall-Petch equation, Cottrell¹² analysed the process by which a crack is formed along the junction of two intersecting slip planes and derived the well known Cottrell equation for brittle fracture. He stated that the ductile-to-brittle transition temperature (DBTT) occurs when;

$$\sigma_y k_y d^{1/2} > \beta \mu \gamma \quad \text{..... (2.2)}$$

where μ is the shear modulus;

γ is the effective surface energy of a crack; and

β is a constant ($= 1$).

Increases in k_y , σ_y , σ_i , and d all make the metal brittle. Cottrell¹² suggested that there are two sources of weakness which lower the surface energy γ of the material: stress concentrations and chemical agents in grain boundaries or on crack faces. Notches result in a stress concentration at the root of the notch and have been shown to change the variable β from $\beta = 1$ for uniform, uniaxial tension, to $\beta = 1/3$ for plastically constrained, notched samples. Of the variables in the Cottrell equation, k_y is considered to be the most important since it determines the number of dislocations released into a slip band when a dislocation source is unpinned.

This factor (k_y) may depend upon alloy content, test temperature, or heat treatment¹³.

Tetelman and McEvily¹⁴ have listed three important stages associated with the slip or twin-nucleated cleavage fracture of a polycrystalline aggregate. They are:

1. the nucleation of a crack by shear stresses τ_N ;

2. the initial growth of the crack under tensile stresses σ_B ; and
3. the traversing of the first strong barrier that the crack encounters σ_B .

The cleavage fracture stress (σ_f) of a material will be that stress at which the most difficult of these steps is overcome. These steps are illustrated in Figure 2.2. It was suggested that the difficulty of each step depends on "cleanliness" which is directly related to the distribution of second phase particles in the material. Dirty materials have been defined as those which contain inhomogeneous distributions of particles and impurity atoms (often at the grain boundaries), and clean materials as those in which the material is single phase only, or those in which the second phase is homogeneously distributed. Thus, even high purity material may be regarded as dirty using this definition.

The mode of deformation which operates will affect the fracture mechanism. Figure 2.3 illustrates that the yield stress for slip or twinning varies with temperature¹⁴. The twinning stress is relatively independent of temperature, whereas that for slip varies greatly. It may be observed that at low temperatures the stress required for twinning is less than that required for slip, and twinning is the preferred mode of deformation. The opposite is true at higher temperatures.

A large stress concentration will develop at the tip of a slip band or twin if it is blocked by a strong obstacle such as a grain or phase boundary. If this concentrated stress is not relaxed by a plastic deformation process, a crack will form. The work done in crack nucleation, γ_m , decreases:¹⁴

1. when few sources exist around the incipient crack (heavy pinning);
2. when the slip or twin band which concentrates the stress forms rapidly, so that relaxation does not have time to occur; or
3. when the crack is formed at a low temperature.

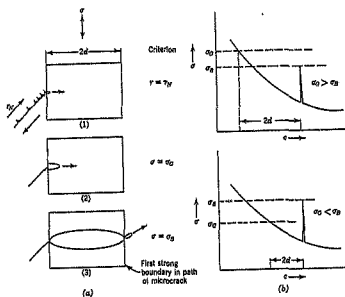


Figure 2.2 a) Three stages associated with the development of an unstable cleavage fracture in a polycrystalline metal. In single crystals only stages (1) and (2) are present.

b) Conditions under which non-propagating microcracks are not formed (1) and are formed (2) in a polycrystalline metal.¹⁴

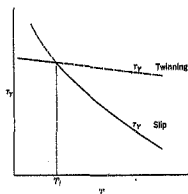


Figure 2.3 Effect of test temperature on the critical resolved shear stress $\bar{\tau}_y$ for slip and twinning in a typical BCC metal. Yielding occurs by twinning when $T < T_c$ and by slip at $T > T_c$ ¹⁴

Hard phases at grain boundaries do not permit much relaxation of the concentrated stresses, and thus crack nucleation will occur more easily. The size and shape of a particle affects the probability for crack nucleation. Shorter particles may allow for the activation of sources above and below them and thus accommodate deformation. In addition, if the particle-matrix interface is able to break, voids will form and coalesce to form a fibrous crack. This will increase the strain rate at the crack tip, and cleavage cracks may be formed ahead of the fibrous crack, resulting in a mixed fracture.

Pollard⁹ stated that the effect of carbon and nitrogen on ferritic stainless steels depends on whether they are in solution or precipitated. In solution they reduce dislocation mobility and hence raise σ_y and reduce the fracture stress (σ_F). Precipitating carbon and nitrogen from solution reduces σ_y , but the effect on σ_F depends on the precipitate morphology. Grubb and Wright¹⁵ found that the intragranular plate-like precipitates (which they concluded to be Cr_2N) were particularly embrittling.

McMahon and Cohen¹⁶ hypothesized on the formation of a cleavage microcrack in ferrite in the following manner. A crack starts in a brittle precipitate after some deformation of the ferrite matrix and propagates across the precipitate as a Griffith crack. If the ferrite is unable to yield, it will accept the crack as a Griffith flaw. Alternatively, if the ferrite can yield locally by slip or twinning, a microcrack will not form in the ferrite. Veistinen et al¹⁷ found that the initiation of cleavage is impossible when the precipitates are loosened from the matrix as opposed to them cracking.

Pollard⁹ has shown that an increase in chromium from 26 to 35% severely reduces weld ductility due to an increase in σ_y and a reduction in σ_{fas} as a result of substitutional hardening. This is a direct result of the reduced interstitial solubility with increasing chromium content. This differs from the findings of others who found no change,¹³ or a toughening effect⁴ with increasing chromium content. The variation in results is probably due to

experimental variables such as gauge (specimen thickness), grain size, and interstitial content.

Several investigations have been dedicated to the relationship between twinning and the brittle fracture of bcc metals. Grubb and Wright¹⁵ found that twinning of Fe-26%Cr alloys was generally favoured by reduced interstitial content and increased solid solution alloying. They concluded that twinning is usually associated with slip difficulties and corresponding flow stress increases. Reid¹⁸ looked at the relationship between twinning and brittle fracture of bcc metals and found cases where:

1. twinning and brittle fracture were independent responses;
2. a propagating crack may nucleate a twin; and
3. twins may nucleate cracks.

Thus, deformation of bcc metals by twinning need not be associated with reduced toughness.

It has been shown that the transition temperature of ferritic stainless steels is a function of gauge^{19, 20}. Wright²⁰ found this phenomenon in Fe-26%Cr-1%Mo alloys. The lower transition temperatures measured for the lighter gauges were attributed to a finer grain size, as a result of hot and cold work, and to a greater role of plane stress (as opposed to plane strain) fracture mechanics. Nichol¹⁹ found the same gauge-related DBTT effect in Fe-29%Cr-4%Mo-2%Ni steels. His results of Fracture Appearance Transition Temperature (FATT) versus sample thickness are shown in Figure 2.4.

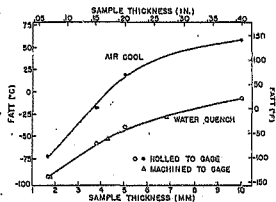


Figure 2.4 Effect of sample thickness and cooling rate from an 1121 °C, 30 min-anneal, on the Fracture Appearance Transition Temperature (FATT)¹⁹

Ashby and Embury²¹ have developed a model for the behaviour of dislocations adjacent to a crack tip, and the way in which the DBTT depends on dislocation density, and therefore on prior plastic working. Their model shows that if dislocations are always within the crack-tip field so that they may move and multiply, a high energy fracture will occur. Thus, there exists a critical dislocation density (ρ_c) below which a crack will run without capturing dislocations. As the dislocation density increases, work hardening eventually makes the dislocations harder to move, and plasticity and blunting are inhibited. These relationships are shown in Figures 2.5 and 2.6. This model indicates that an optimum in ductility and DBTT of bcc metals will be reached when in a material condition intermediate between fully recrystallized and fully worked.

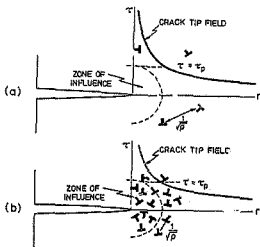


Figure 2.5 Schematic showing how the crack tip field may be unable to capture dislocations and cause them to multiply when the dislocation density is low, but may do so when the dislocation density is higher.²¹

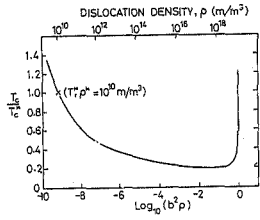


Figure 2.6 The variation of the ductile-brittle transition temperature with dislocation density.²¹

2.3 Interstitials - Content and Form

In 1951, Hochmann³ and Binder and Spendelow⁴ first showed that the lowering of the impact strength of ferritic chromium steels as the chromium content is raised above about 20% chromium is not due to chromium alone, but is associated mainly with the carbon and nitrogen contents. They also concluded that of itself, chromium has a strong toughening influence on the ferrite matrix, but the tolerance for carbon and nitrogen decreases as the chromium content is increased.

To better understand the effects of carbon and nitrogen on ferritic alloys, Pollard²² analysed the solubility of carbon and nitrogen for an Fe-26%Cr steel (Figure 2.7). It was found that;

1. all nitrogen was in solution above 927 °C;
2. the precipitation of nitrides occurred from 927 to 592 °C;
3. the addition of titanium lowered the soluble nitrogen level at all temperatures; and
4. carbon solubility was lower than nitrogen solubility below 1038 °C.

The solubility of interstitial elements can be used to explain the effects of heat treatment on the toughness of these alloys. For example, Plumtree and Gullberg¹³ have shown that the ductile-to-brittle transition temperature (DBTT) of high chromium ferritic alloys is directly related to the volume of second phase particles, which increases with an increase in interstitial content. In addition Semchysen et al²³ found that nitrogen alone is less harmful than carbon. This is probably due to the variation in solubility limits, and the formation of different precipitates. Pollard²² identified the precipitates in Fe-26%Cr steels using X-ray diffraction. With a high nitrogen and low carbon level the precipitate formed was found to be Cr₂(C,N), whereas with a low nitrogen and high carbon level the precipitate formed was Cr₂₃C₆.

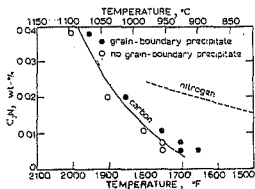


Figure 2.7 Solubility of carbon and nitrogen in 26% chromium steel versus temperature.²²

2.4 Stabilization

A common approach to reducing the deleterious effects of carbon and nitrogen is to precipitate them in a more stable form than that of chromium carbonitrides. Titanium and/or niobium are often used, and form $Ti(C,N)$ or $Nb(C,N)$.

Demo²⁴ suggested three methods to control interstitials in high chromium ferritic steels:

1. Maintain the interstitials (C+N) below critical levels. It was found that to achieve as-welded ductility at 2.5mm gauge, (C+N) limits were 200 p.p.m. for Fe-26%Cr and 20 p.p.m. for Fe-35%Cr.
2. Use weld-ductilizing additives such as aluminium, copper, platinum, palladium, or silver.
3. Use gettering additives such as titanium or niobium which form stable carbides and nitrides.

It was stated that combined additions of titanium (or niobium) and

aluminum give the best as-welded ductility. In his patent²⁵, Demo suggested that the carbon and nitrogen contents of the alloys are being 'neutralized' by these alloying additions. Semchysen et al²³ also concluded from their work that titanium carbonitrides and to a lesser extent niobium carbonitrides are less harmful to the toughness of ferritic stainless steels than chromium carbonitrides. The reasons for this were explained by Pollard²² who proposed that stabilization prevents grain-boundary precipitation by the formation of titanium carbonitride randomly in the molten steel, which serve as nuclei for the formation of other precipitates within the grains.

Semchysen et al²³ found that titanium alleviated the deleterious effects of high-temperature exposure on ductility, which occurs in processes such as welding. Otherwise, the titanium-modified alloys exhibited DBTT Values commensurate with their (C+N) contents. In the same way, Wright²⁶ concluded that the effect of stabilization on as-welded toughness was greater than the effect on the baseplate toughness.

Grubb et al²⁷ stated that titanium promotes intergranular fracture and embrittles very low interstitial-containing ((C+N) < 100 p.p.m.) ferritic alloys. It was suggested that the cause of intergranular fracture in stabilized ferritic alloys is the segregation of oxygen to the grain boundaries, which lowers γ^{28} . This is probably a result of the getting of carbon, as carbon in solution has been shown to reduce the embrittlement produced by oxygen.

The amount of stabilizing elements added to ferritic alloys has been shown to be crucial, as 'over-stabilizing' also embrittles the alloys 13 23 24 26. Wood²⁹ studied the effects of residual elements on the mechanical properties of an Fe-18%Cr steel and found that residual titanium (i.e. above that required to stabilize the (C+N) content) was the most potent solid solution strengthening element. Pollard⁹ suggested that a maximum weld ductility was achieved in vacuum-melted ferritic alloys when titanium, niobium, or zirconium were added at one to two times the stoichiometric equivalent of the (C+N) content. It was also shown that amounts greater than that suggested resulted in decreased ductility due to dispersion strengthening.

In their patent, Sipos et al³⁰ listed several groups of additives which have been found effective in preventing postwelding brittleness in ferritic alloys containing 28 to 37% chromium. (It should be noted that even in this case it was suggested that carbon and nitrogen levels were maintained below 0.03 and 0.04 respectively, and actually recommended even lower levels of 0.01 and 0.015).

The additives are listed in Table 2.1.

TABLE 2.1 Effective postwelding brittleness preventers for high-chromium ferritic alloys³⁰.

Group 1 -	Al, 0.1 to 0.9%
Group 2 -	Cu, 0.3 to 1.3%
Group 3 -	Al, 0.1 to 0.5% together with Cu, 0.4 to 1.3%
Group 4 -	Al, 0.1 to 0.5% together with Cu, 0.3 to 0.7% together with V, 0.1 to 0.3%
Group 5 -	Al, 0.1 to 0.5% together with Ag, 0.03 to 0.05%
Group 6 -	Al, 0.1 to 0.5% together with V, 0.1 to 0.35%
Group 7 -	Pt, 0.2 to 1.0%
Group 8 -	Pd, 0.2 to 1.0%
Group 9 -	Ag, 0.1 to 1.0%

Redmond³¹ has shown that the stabilizing element used in 18%Cr - 2%Mo stainless steel strongly affects the weld microstructure. In the presence of niobium (or niobium and aluminium) the weld microstructure consisted of long columnar grains with a very distinct centre-

line. If titanium was used, the fusion zone contained equiaxed grains. Consequently, the titanium stabilized weldment exhibited better impact toughness than the niobium-stabilized weldment, while the baseplate impact toughness showed the opposite effect. This is probably due to the microstructural effect. The niobium-stabilized steel to which 0.5% aluminum had been added gave the lowest impact transition temperatures in both the base metal and the weld metal.

2.5 High-Temperature Embrittlement

When high chromium ferritic stainless steels containing relatively high interstitial levels are heated above approximately 1000°C, they subsequently experience a severe loss in toughness and ductility at room temperature. This phenomenon is known as high-temperature embrittlement. Experimental work has shown that toughness of the high chromium ferritics is a function of:

1. interstitial content^{13 15 19 22 23 32-34};
2. chromium content^{22 23};
3. heat treatment²⁹⁻³⁵;
4. the morphology of the precipitates^{15 19 22 23 32-34}.

Grubb and Wright¹⁵ studied Fe-26%Cr alloys with two different combined (C+N) levels. It was found that the precipitation of carbon and nitrogen in the low interstitial alloys (C+N = 67 p.p.m.) was directly related to the brittleness of the material. Therefore, quenching from high temperatures to suppress precipitation resulted in the lowest DBTT, while furnace cooling from the same high temperatures, which allowed precipitation to occur, embrittled the material. Conversely, the same high temperature quench for the high interstitial alloy (C+N = 570 p.p.m.) produced embrittlement. This variation in effect is related to the state of the carbon and nitrogen^{13 15 19 22 23 32-34}.

Pollard²² found that the loss of ductility in low (C+N) Fe-26%Cr alloys coincided with the appearance of grain-boundary carbonitrides. In the same way, Wright²⁶ stated that 'the effect of solute (C+N) in low (C+N) ferritic stainless steels seems to be quite benign in comparison with the effect of carbide and nitride precipitates'.

All conclusions point to the fact that high-temperature embrittlement of high-chromium ferritic stainless steels is due to precipitation of carbides and nitrides as a result of the relief of supersaturation³¹ when these alloys are heated to high temperatures^{31 35}. The low interstitial alloys will suffer from little or no supersaturation and thus quenching will suppress precipitation and thereby toughen the material, whereas slow cooling or low temperature anneals will allow the embrittling carbonitrides to form.

Using transmission electron microscopy, Demo³² found that high interstitial-containing alloys quenched from 1100 °C had precipitates on nearly all the dislocations. It was concluded that these alloys were embrittled in a manner similar to precipitation hardening. When these same alloys were reheated to 850 °C or slow cooled from 1100 °C the alloys became ductile and it was observed that the dislocations were precipitate-free. It was proposed that with more time available, migration of carbon and nitrogen had resulted, and precipitation had occurred on the higher energy surfaces of the grain boundaries. Similarly, Levanova et al³³ have shown that the post-weld ductility of high-chromium ferritic steels is dependent upon the heat input (ie. temperature and rate of cooling) which is analogous to high-temperature embrittlement.

2.6 475 °C Embrittlement

Ferritic stainless steels which contain more than approximately 10% chromium may become embrittled after long time exposures in the temperature range 400 to 550 °C. This embrittlement is most severe at 475 °C and is therefore referred to as 475 °C (or 885 °F) embrittlement. The embrittled alloys exhibit a severe loss in toughness and elongation and an increase in both strength and hardness.

Prior to 1951, many studies were carried out and 475 °C embrittlement was believed to be related to α -phase formation. Subsequently, however, Williams³⁶ and Williams and Paxton³⁷ first proposed the existence of a miscibility gap in the iron-chromium equilibrium diagram below the α -phase region in which alloys separate into iron-rich and chromium-rich bcc phases. Their revised equilibrium diagram is shown in Figure 2.8.

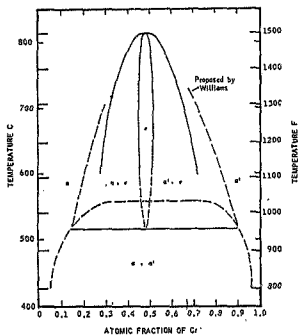


Figure 2.8 Phase diagram of the iron-chromium system according to Williams³⁶.

Fisher, Oulfs and Carroll³⁸ reported that the composition of the chromium-rich phase ranges from 61 to 83% chromium. There exists a spinodal within the miscibility gap and the mode of precipitation of α' is dependent on temperature and composition. Nicol, Datta and Aggen³⁹ confirmed that the onset of 475 °C embrittlement in 26 and 29% chromium alloys was accompanied by a clustering of chromium atoms along the {100} planes, indicative of spinodal decomposition. Concurrently, the deformation mode was found to change from turbulent slip to planar slip along {110} matrix planes.

DeNys and Gielen⁴⁰ found the decomposition of an Fe-20%Cr alloy at 470 °C to occur by nucleation and growth, while binary iron-chromium alloys containing 30, 40 and 50% chromium decomposed *spinodally*. Thus, it appears that spinodal decomposition is favoured by high chromium contents and low aging temperatures³⁹, while the nucleation and growth mode will occur outside the spinodal²⁶.

The kinetics of formation of α' increase with increased alloying and cold work, and decrease with increasing purity^{26 35 39 41}. Demo³⁵ has summarised the effects of composition on 475 °C embrittlement of iron-chromium alloys (Table 2.2).

TABLE 2.2 Effects of composition on 475 °C embrittlement in chromium-iron alloys³⁵

ELEMENT	EFFECT ON 475 °C EMBRITTLEMENT
Cr	Intensifies
C	No effect; intensifies
Ti, Nb	Intensifies
Mn	Lowers slightly
Si	Intensifies
Al	Intensifies
Ni	Low amounts; intensify Large amounts; decrease
N	Very slight; intensifies
P	Intensifies
Mo	Intensifies
Severe cold work	Intensifies

Although the existence of the σ -phase is well established there is still controversy concerning its role in 475 °C embrittlement. Grobner⁴¹ reported that the 475 °C embrittlement of 14 and 18% chromium ferritic stainless steels was caused by precipitation of α' on dislocations. Others have attributed the embrittlement to the formation of deformation twins.^{26 39} However, Yasunaka et al⁴² stated that although twinning contributed to embrittlement through microcrack nucleation, the intrinsic cause of 475 °C embrittlement is the change

of slip mode, a restriction of cross slip, and the resulting ease of cleavage crack formation. Further, Grubb et al²⁷ found no sub-critical microcrack formation in an embrittled Fe-26%Cr alloy, and thus inferred that α' precipitation greatly increased the flow stress.

The occurrence of 475 °C embrittlement in ferritic stainless steels is dependent upon time, temperature, composition, and cooling rate. The effects of embrittlement are reversible by heating the embrittled alloys above 550 °C for a sufficient length of time. Demo³⁵ suggested that 475 °C and σ -phase embrittlements are not related metallurgically, and significantly shorter exposure periods can produce 475 °C embrittlement as compared to σ -phase embrittlement. Thus high chromium alloys should not be used for extended service between 400 and 550 °C, and should be fast cooled through this temperature range to avoid embrittlement.

2.7 Sigma-Phase Embrittlement

Reference to the iron-chromium phase diagram (Figure 2.8) reveals an intermediate σ -phase at approximately 50% chromium. Sigma-phase is a hard, brittle intermetallic compound with the approximate composition FeCr. It has a tetragonal unit cell, with a c/a ratio of 0.52.⁴³ Bain and Griffiths⁴⁴ suggested the existence of a compound in the iron-chromium system at about 50% chromium, as early as 1927.

Demo³⁵ reported that σ has been found to form in alloys with as little as 20% and as much as 70% chromium when exposed to temperatures between 500 and 800 °C. However, Wright²⁶ extended the upper limit of formation to 900 °C. Redmond et al⁴⁵ found that σ precipitation in an Fe-18%Cr alloy (containing 0 to 5% Mo) displayed C-curve kinetics with the nose at 800 to 850 °C. Sigma-phase formation is enhanced by cold work^{26 38} and alloying with elements such as molybdenum, nickel, manganese, silicon, niobium and titanium^{26 35 45}. These factors will thus change the time and temperature dependence of σ -phase formation.

Once nucleated, σ -phase grows very rapidly, with its growth causing an increased dislocation density at the α - σ interface.⁴⁵ The general tendency is for σ to form at the ferrite grain boundaries²⁶ and thereby embrittle due to an increase in the stress concentration, or a decrease in the effective surface energy of a crack (γ). Fracture of σ -phase embrittled ferritic stainless steels then occurs by intergranular fracture.¹⁹ Similar to 475 °C embrittlement, the effects of σ -phase embrittlement are reversible and may be dissolved by heating an embrittled alloy above the σ formation temperature for an hour or more.³⁵

2.8 The Rhenium Ductilizing Effect

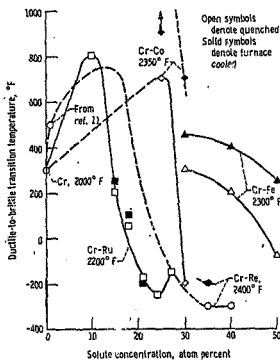
Iron has been found to improve the low temperature ductility of unalloyed chromium due to a phenomenon known as the rhenium ductilizing effect.

This was discovered as early as 1955 when Geach and Hughes⁴⁶ observed improved low-temperature ductility in W-25%Re and Mo-35%Re alloys, as compared with unalloyed tungsten and molybdenum. It was later shown by Klopp et al⁴⁷ that Cr-35%Re exhibited similar improvements in low-temperature ductility. Thus, the 'rhenium ductilizing effect' was found to be common to all three Group VIB elements (Cr, Mo, W).

Several alloy systems, including the chromium-iron system, have been found to be rhenium analogues. The addition of rhenium and its analogues (such as iron) appears to reduce the ease of crack propagation compared with unalloyed chromium. Although the phenomenon is not well understood, 'it is known that twinning is enhanced, the slip systems are modified, and both the strain-rate and temperature sensitivity of the yield stress are decreased'.⁴⁸

Stephens and Klopp⁴⁹ found that as the alloy composition approached the maximum solubility in chromium (for the chromium-cobalt, chromium-ruthenium and chromium-rhenium systems) or the σ composition (for the chromium-iron system) a sharp decrease in ductile-to-brittle

transition temperature was observed (Figure 4.1). The lowest DBTT found for the chromium-iron system was at Cr-50 at % Fe (~ Cr-54 wt % Fe) in addition, Klopp⁵⁰ has found that in the case of chromium-cobalt and chromium-iron, the alloys must be quenched from the single phase region in order to exhibit the twinning and low temperature ductility. In contrast, the chromium-rhenium and chromium-ruthenium systems are not dependent upon cooling rate.



Note: 2000 °F = 1093 °C
 2200 °F = 1204 °C
 2300 °F = 1260 °C
 2350 °F = 1285 °C
 2400 °F = 1315 °C

Figure 2.9 Effects of solute content on ductile-to-brittle bend transition temperature of chromium alloys annealed at indicated temperatures. After Stephens and Klopp⁴⁹

Several common characteristics of solutes promoting the rhenium ductilizing effect have been identified. These are⁵⁰:

1. the ductilizing solutes are from Groups VIIa and VIIIa of the periodic table;
2. the ductilizing solutes form intermediate σ -phases with chromium;
3. the ductilizing solutes have relatively high solubilities in chromium; and
4. maximum cold ductility occurs in saturated or supersaturated single-phase, solid solution alloys.

Stephens and Klopp⁴⁹ have postulated the mechanism by which these characteristics contribute to reducing the DBTT as follows:

1. a high solubility and a composition near the maximum solubility favour a metastable structure with respect to σ precipitation, and
2. during quenching or straining at lower temperatures, the metastable structure produces localized stresses and thus acts as a dislocation and twin source with a resulting lowering of the DBTT.

2.9 Summary

The factors which can affect the mechanical properties of ferritic stainless steels have been presented in the literature survey. The majority of results discussed relate to 20 to 30% chromium steels. The effects of the parameters will probably differ for the Fe-40%Cr steel of the present study. This will be examined. The effect of an increase in chromium on ductility has not been conclusively discovered, due to variations in experimental parameters. Finally, the rhenium ductilizing effect is not a well understood phenomenon. The alloy of the present study appears to be approaching the composition for the optimum ductility resulting from this phenomenon.

3. EXPERIMENTAL PROCEDURE

3.1 Melting Practice

A considerable amount of experimentation was performed to obtain vacuum induction-melted ingots with the desired purity. In particular, the aim was to keep the interstitial elements (C, N, and O) to a minimum. All of the alloys were melted in a Leybold Heraeus vacuum induction melting unit at The Council for Mineral Technology (MINTEK). A detailed account of all the different procedures carried out is beyond the scope of this dissertation, therefore only a brief summary will be presented here. Electrolytic iron and chromium were used as base materials, with compositions as listed in Table 3.1. The purity of the starting materials was found to be a major factor in obtaining high-purity final alloys.

TABLE 3.1

The compositions of the electrolytic iron and chromium as reported by the manufacturers. (All maximum values) (wt.%).

ELEMENT	IRON	CHROMIUM
C	0.003	0.05
N	0.003	0.02
O	0.05	0.05
Al	0.003	0.015
Si	0.005	0.04
N.	0.007	
Cu	0.001	
P	0.003	
S	0.003	0.01
Sn	0.006	
Fe	BALANCE	0.35
Cr	0.002	99.5

The melting parameters which were considered were time, temperature and pressure. All ingots had a nominal composition of 60% Fe - 40% Cr. The melting practice which yielded good results and which was then adopted for the production of all the experimental alloys, consisted of the following steps. The electrolytic iron and chromium were charged into a magnesia crucible. The temperature within the furnace was raised to between 900 and 1000 °C with the lowest obtainable pressure. This pressure was normally in the region of 4Pa. The metal was held at this temperature and pressure for 45 minutes in order to allow solid state diffusion of the gases from the raw materials, as well as outgassing of the crucible. The furnace was then backfilled with argon to a pressure of 1kPa. At the same time the power was increased so that the metal became molten. The temperature of the molten metal was kept below 1700 °C, and was normally in the range of 1610 °C to 1570 °C. Temperature measurements of the metal were made through the furnace viewing glass using a Williamson pyrometer. When the metal became molten it was immediately tapped into mild steel moulds. A tapping temperature of 1610 °C was found to be optimum for pouring and also to prevent adhesion of the metal to the mould. The metal was cooled under a pressure of approximately 4Pa.

The melting and tapping of the metal were carried out as quickly as possible in order to avoid contamination by gases. This exercise normally took less than 10 minutes.

3.2 Fabrication

Preliminary experimental work was performed on 4 melts each of 4 kg mass. For the purposes of this study, the compositional variations of these melts were taken to be minimal. The actual analytical compositions are listed in Table 3.2.

TABLE 3.2

The composition of the preliminary experimental melts.

ELEMENT	INGOT DESIGNATION			
	VF 44	VF 45	VF 46	VF 47
C	0.005	0.004	0.006	0.006
N	0.005	0.004	0.005	0.005
Cr	39.0	38.4	38.8	38.6
Al	0.019	0.019	0.017	0.018
Mn	0.01	0.01	0.01	0.01
Si	0.035	0.037	0.035	0.036
P	0.008	0.008	0.007	0.008
S	0.005	0.005	0.005	0.005
O	0.085	0.10	0.095	0.10
Fe	BALANCE	BALANCE	BALANCE	BALANCE

The ingots were rolled from an initial 45mm down to 6mm thickness, using a 50 ton, 2-high reversing rolling mill. The ingots were initially soaked at 950 °C for one hour, then rolled until the temperature dropped to 650 °C. They were then placed back in the furnace at 950 °C for 20 minutes, and the rolling sequence was repeated. A digital pyrometer was used to determine the temperature during rolling. A soaking time of 20 minutes at 950 °C between rolling sequences had previously been determined to be sufficient to allow the ingot to return to 950 °C. (This had been found using a thermocouple positioned in the centre of one experimental ingot.)

If the material started to bend during rolling, it was straightened using a 100 ton forging press, then immediately returned to the furnace. When the final thickness of 6mm was obtained, the material was quenched in water.

3.3 Heat-Treatment and Specimen Preparation.

The rolled plate was cut into two or three sections which were then heat-treated at temperatures between 700 and 1300 °C for one hour, and water quenched. The heat treatment temperatures and the ingot from which the sections were taken are listed in Table 3.3.

TABLE 3.3 Heat treatment temperatures

SAMPLE NUMBER	1 HOUR AT TEMPERATURE (°C)	INGOT DESIGNATION
1	700	VF 47
2	750	VF 45
3	800	VF 44
4	850	VF 47
5	900	VF 45
6	950	VF 46
7	1000	VF 44
8	1050	VF 47
9	1100	VF 46
10	1200	VF 45
11	1300	VF 44

From each heat-treated section, tensile test specimens with a 25mm gauge length and a cross-section of 6.25 by 5mm were made, with their length parallel to the rolling direction, and half-size Charpy V-notch impact specimens (5 x 10 x 55mm) were made with their length transverse to the rolling direction.

A holder was constructed for the automatic polishing equipment so that the 10 x 55mm side of 18 Charpy impact specimens could be polished at one time. After notching, these were polished to a 1µm finish. It was then possible to observe the deformation mechanisms on the polished surfaces after fracture.

3.4 Mechanical Testing

Ductile-to-brittle transition temperatures (DBTT) were measured using a 50kN ESH servohydraulic machine by slow-bend testing at a cross head rate of $8.3 \times 10^{-2} \text{mm s}^{-1}$. The sample geometry was identical to that of the Charpy V-notch impact specimens.

To achieve the desired test temperatures, baths containing dry ice in iso-propyl alcohol were used for tests below 22°C , and water was used for tests above 22°C . Load-deflection curves were recorded at the various test temperatures. These curves were analysed according to the methods of Edwards et al⁵¹. DBTT values were measured as:

1. the area under the curve to maximum load as a function of temperature; and
2. the total area under the curve as a function of temperature.

A "Simpsons rule" computer programme was used to analyse the areas under all the curves. These methods, and the fracture appearance transition temperature (FATT) gave similar DBTT values.

Charpy V-notch impact tests were carried out at ambient temperatures for all the heat treatments, using a Tinius Olsen impact machine.

Tensile tests were also carried out for all heat treatments at ambient temperatures, using an Instron 1175 tensile testing machine and a cross-head velocity of $3.3 \times 10^{-2} \text{mm s}^{-1}$. Hardness measurements were made using a Vickers pyramid diamond indenter with a 30kg load.

3.5 Metallurgy

Samples from each heat treatment were mounted for metallographic examination in both the longitudinal and transverse directions, i.e. parallel to and perpendicular to the rolling direction. A few passes of the specimen on a lum diamond polishing wheel were necessary to

remove a passive surface before etching. These were then etched in glyceric acid (which consists of 30ml glycerine, 50ml concentrated hydrochloric acid and 10ml concentrated nitric acid). The samples were dip etched for approximately 50 seconds, rinsed in water and alcohol and hot-air dried. Grain size determinations were carried out after etching. The precipitate morphology and location were observed both before and after etching.

The same metallographic techniques were also used for specimens in the as-cast condition in order to estimate visually changes in the quantity of precipitates present subsequent to the use of different melting techniques.

The mounted samples of each heat treatment were repolished and etched in order to determine if σ -phase was present. The specimens were etched for five seconds in boiling ferricyanide solution which consists of 30g $K_3Fe(CN)_6$, 30g KOH and 60 ml H_2O . This etchant stains ferrite yellow, and σ -phase blue. Sigma-phase was also identified using scanning electron microscopy in the backscattered mode, and energy dispersive X-ray (EDX) analysis. As a final verification, σ -phase was extracted from the matrix of a sample which had been held at 750 °C for several hours. Sigma-phase was positively identified by X-ray diffraction using the Debye-Scherrer method.

The volume percent of precipitates was analysed for samples from all 11 heat treatments using a TAS Leitz image analyser. Sixty fields of view were used for each specimen.

A qualitative energy dispersive spectroscopy (EDS) investigation was carried out using a JEOL Super-probe to determine the elements present in the precipitates of samples heat-treated at 700 and 1050 °C. These specimens were selected to give an overall view of precipitation, by considering a low and relatively high heat treatment temperature. It was necessary to carbon coat the samples prior to analysis in order to comply with the standards used.

In order to examine the dislocations and precipitates, Samples 1, 8 and 11, heat-treated for one hour at 700, 1050 and 1300 °C respectively, were prepared for transmission electron microscopy. Rods of 3.1mm diameter were machined from broken Charpy specimens. Discs of approximately 1mm thickness were cut from these rods. These were mechanically polished to approximately 80µm thickness, then jet polished to perforation using a Struers Tenupol at 70V and a low flow rate (setting < 1). The electrolyte used was 5ml perchloric acid, 95ml glacial acetic acid and 1ml of chromic acid. The addition of 2ml alcohol per litre of solution was necessary to reduce the chromium to Cr⁺³.

3.6 Fractography

The polished surfaces of both the slow-bend and the Charpy V-notch impact specimens were observed after fracture, using both optical and scanning electron microscopy, in order to identify the deformation and fracture mechanisms.

The fracture surfaces of the tensile specimens, the Charpy V-notch impact specimens and the slow-bend specimens were observed using an optical microscope. Several of the Charpy impact and slow-bend specimens were examined further using the SEM in order to obtain more detailed information on the fracture mechanisms.

3.7 Alloyed Fe-40%Cr

A further 14 ingots of Fe-40%Cr were made using the procedure outlined previously in Section 3.1. Of these, 13 ingots were alloyed with various elements in order to observe the different effects of these additions on the mechanical properties. The remaining ingot (A) was a base Fe-40%Cr alloy which was used as a standard for comparison. The compositions of these alloys are listed in Table 3.4. The niobium, ruthenium and nickel were added in the crucible with the electrolytic iron and chromium. Aluminium and titanium additions were made immediately prior to pouring the molten metal. The Al and/or Ti were placed in pure iron foil attached to the end of

Table 3.4 Composition of alloyed Fe-40%Cr

Alloy	C	N	O	S	P	Si	Mn	Other	
								Analysis	Addition
A	0.003	0.002	0.056	0.007	0.003	< 0.01	< 0.04	-	-
B	0.010	0.003	0.100	0.007	0.003	0.03	< 0.04	0.20 Nb	0.2 Nb
C	0.003	0.009	0.040	0.006	0.003	< 0.01	< 0.04	0.07 Ti	0.2 Ti
D	0.010	0.002	0.029	0.006	0.003	0.03	< 0.04	0.12 Al	0.2 Al
E	0.006	0.003	0.080	0.005	0.004	0.03	< 0.04	0.19 Ru	0.2 Ru
F	0.011	0.004	0.046	0.006	0.004	0.04	< 0.04	0.03 Ti + 0.20 Ru	0.1 Ti + 0.2 Ru
G	0.017	0.002	0.076	0.005	0.004	0.04	< 0.04	2.0 Ni	2.0 Ni
H	0.006	0.002	0.043	0.006	0.002	< 0.04	< 0.04	0.02 Ti	0.05Ti
I	0.010	0.002	0.041	0.006	0.002	< 0.04	< 0.04	0.19 Ru + 0.02 Ti	0.2 Ru + 0.05Ti
J	0.007	0.002	0.050	0.006	0.002	< 0.04	< 0.04	0.1 Nb	0.1 Nb
K	0.008	0.002	0.008	0.006	0.002	< 0.04	< 0.04	0.02 Al + 0.09 Nb	0.2 Al + 0.1 Nb
L	0.006	0.002	0.044	0.007	0.002	< 0.04	< 0.04	0.98 Ni	1.0 Ni
M	0.008	0.002	0.012	0.005	0.002	< 0.04	< 0.04	0.02 Al + 2.00 Ni	0.2 Al + 2.0 Ni
N	0.007	0.002	0.044	0.004	0.002	< 0.04	< 0.04	0.17 Ru + 2.02 Ni	0.2 Ru + 2.0 Ni

a poker to allow rapid addition. The elements were added in their pure form as Ti bar, Nb chips, Al wire, Ru sponge and Ni briquettes.

The ingots were rolled to plate with a final 12mm thickness using the same procedure as outlined in Section 3.2, with the exception that the soaking temperature (and the initial rolling temperature) was 1050 °C, as opposed to the previous temperature of 950 °C. The material was water-quenched subsequent to rolling. Twelve standard Charpy V-notch samples (10 x 10 x 55mm) and 3 tensile samples with a 50mm gauge length and a 12.5mm x 10mm cross-section were machined from each plate. The Charpy specimens were cut with their length transverse to the rolling direction, and the tensile specimens had their length in the longitudinal direction. All test pieces were heat-treated for one hour at 1050 °C in an argon atmosphere, then water-quenched.

The Charpy V-notch impact DBTT was determined for each alloy. Test temperatures were maintained in the same way as outlined in Section 3.4. Ambient temperature tensile tests were carried out with a cross head velocity of $3.3 \times 10^{-2} \text{mm s}^{-1}$ and Vickers hardness tests were also performed.

Again, samples of each alloy were mounted, polished and etched for α -phase identification.

4. RESULTS

4.1 Metallography

When considering the microstructure of these high chromium ferritic alloys, and its effect on mechanical properties, three interacting factors must be considered. These are:

1. the grain size;
2. precipitation effects, (such as carbides, nitrides and oxides); and
3. the formation of brittle intermetallic phases.

For the heat treatments carried out in the present investigation, σ -phase was the only intermetallic phase considered to be of consequence.

Etching of the heat-treated samples indicated that σ -phase was present after one-hour anneals in the temperature range 700 to 900 °C. The σ -phase nucleated on grain boundaries and precipitates is shown in Figure 4.1. Very little σ -phase was found for the heat treatment at 900 °C.

These results are in agreement with the known C-curve kinetics of σ -phase formation, with a nose between 800 and 850 °C. Sigma-phase was also found for the sample quenched from 1300 °C. This is believed to be due to the slower cooling rate in the critical temperature range as a result of the high annealing temperature. Sigma-phase has a short incubation period, and once nucleated forms quickly in this high chromium alloy.

The measured ASTM grain sizes are listed in Table 4.1. A range is given for each heat treatment and the underlined value represents the grain size which is most prominent for each sample. The average grain diameter is also listed.



Figure 4.1 Sigma-phase nucleated on grain boundaries and precipitates.

TABLE 4.1 ASTM grain sizes and average grain diameters for heat-treated samples.

HEAT TREATMENT TEMPERATURE (°C)	ASTM GRAIN SIZE	AVERAGE GRAIN DIAMETER (μm)
700	<u>2</u> - 3	165
750	3 - <u>4</u>	100
800	<u>3</u> - 4	115
850	<u>2</u> - 3	165
900	3 - <u>4</u>	100
950	<u>2</u> - 3	165
1000	<u>2</u> - 3	165
1050	<u>1</u> - 2	220
1100	<u>1</u> - 2	230
1200	<u>1</u> - 2	230
1300	very mixed many grains >1	

The samples quenched from 1300 °C had a very mixed grain size and therefore an average value is not meaningful. Some grains with diameters greater than 300 μm were observed in the samples annealed at both 1200 °C and at 1300 °C.

A microprobe was used to qualitatively identify the precipitates present in the samples annealed for one hour at 700 °C and at 1050 °C. These results are listed in Table 4.2.

TABLE 4.2 Microprobe analysis of a random selection of precipitates in Fe-40%Cr heat-treated at 700 and 1050 °C.

HEAT TREATMENTS (°C)	SHAPE	MAJOR	MINOR	TRACE	LIGHT ELEMENTS		
					MAJOR	MINOR	TRACE
700 °	1	Cr			0		C
	2	Cr			0		C
	3	Cr			0		C
	4	Cr			0		C
	5	Cr			Fe	0	C
	6	Cr			Fe	0	
	7	Cr			Fe	0	C
1050 °	1	Cr		Fe	0		
	2	Cr	Fe		0		C
	3	Cr	Fe		0		
	4	Cr			Fe	0	
	5	Cr	Fe		0		
	6	Cr	Fe		0		C
	7	Cr			Fe	0	C

It can be seen that most of the precipitates analysed were oxides of chromium, although some also contained small amounts of iron. The carbon value for some of the precipitates was slightly higher than the value attributed to the applied carbon coating. However, this is not conclusive evidence for the presence of carbon, particularly since only trace amounts were detected.

It should be noted that a variety of shapes and sizes were analysed in an attempt to cover the full spectrum of precipitates. It is likely that a small percentage of the precipitates present in the experimental material were carbides and nitrides, however, there is approximately ten times more oxygen than carbon present in this alloy, thus resulting in the predominance of oxides.

Image analysis was carried out for samples from all eleven heat treatments. The volume percent of precipitates was calculated for each sample (Figure 4.2). It can be seen that for heat treatment temperatures up to 1050 °C, the volume percent of precipitates remains fairly constant in the 1% range. This value drops to approximately 0.6% for heat treatments above 1050 °C.

The distribution of precipitate sizes for the various heat treatments was also determined. The majority of precipitates had sizes ranging between 1.5 and 4.5 μm . The medium precipitate size for all heat treatments was approximately 3 μm .

The Hall-Petch equation:

$$\sigma_y = \sigma_i + k_y d^{-1/2} \quad \dots\dots (2.1)$$

predicts the change in yield stress as a function of grain size. This theory assumes that σ_i , the lattice friction stress, and k_y , which is a measure of the pinning of dislocations, remain constant. However varying amounts of interstitials and precipitates and other

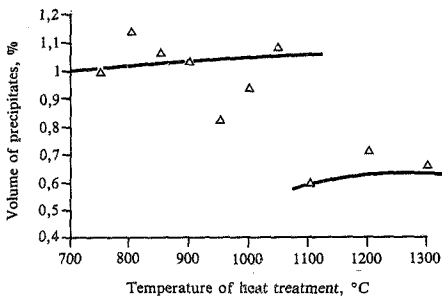


Figure 4.2 Volume percent of precipitates as a function of heat treatment temperature.

second phases, (as well as their size and shape,) will result in a variation in the values of σ_y and k_y . In the present investigation, the yield strength as a function of heat treatment temperature (Figure 4.3) gave a great deal more information than the traditional Hall-Petch plot, due to the three interacting effects of grain size, precipitates, and the presence of σ -phase. Figure 4.3 may be divided into three distinct sections. For heat treatments in the range 700 to 900 °C, the variation in σ_y with temperature is very erratic. Sigma-phase was present in all these samples and this appears to be the dominant factor.

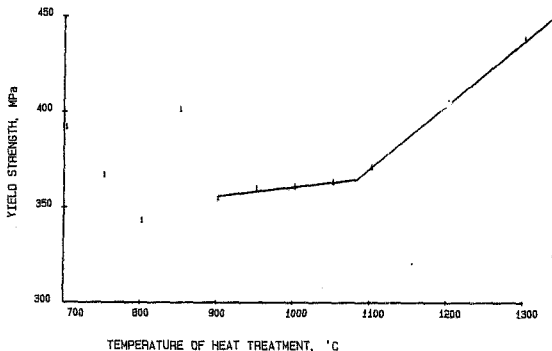


Figure 4.3 Yield strength as a function of heat treatment temperature.

Between 900 and 1100 °C the variation in σ_y with temperature appears constant with a slope of 0.8MPa/°C. The change in σ_y for heat treatment temperatures between 1100 and 1300 °C increases to 0.33 MPa/°C. The increase in yield stress for this high temperature range (1100 to 1300 °C) corresponds with the drop in optically resolvable volume percent precipitates for the same temperature range (Figure 4.2). The increase in yield stress with temperature above 1100 °C, is probably a result of precipitate strengthening as will be discussed later. (see Section 5.5).

4.2 Mechanical Tests

The results of the Charpy V-notch impact tests, the tensile tests and the hardness tests, all carried out at ambient temperatures, are listed in Tables 4.3, 4.4 and 4.5 respectively. The second value listed for several of the impact energies represents a value which deviated greatly from the average. These low energies were often due to the presence of a flaw in the material. Figures 4.4 and 4.5 are plots of the impact energies and of the hardness values as a function of heat treatment temperature.

The ductile-to-brittle transition temperatures (DBTT) are listed in Table 4.6. Tests were only conducted up to 32 °C since it was found that samples with DBTT's above 32 °C contained α -phase.

TABLE 4.3 Ambient temperature Charpy impact energies. (half size specimens).

SAMPLE NO.	HEAT TREATMENT TEMPERATURE (°C)	IMPACT ENERGY (J)
1	700	2.5
2	750	1.8
3	800	3.5
4	850	2.2
5	900	18.3, 4.1 *
6	950	50.3, 7.5 *
7	1000	61.1, 31.9 *
8	1050	63.0
9	1100	65.0, 10.8 *
10	1200	24.4
11	1300	11.7

TABLE 4.4 Ambient temperature tensile test results (20 °C, cross-head velocity: $3.3 \times 10^{-2} \text{mm s}^{-1}$).

SAMPLE NO.	HEAT TREATMENT TEMP. (°C)	Y.S. (MPa)	U.T.S. (MPa)	% El	% R of A
1	700	391.2	507.4	30.5	64.5
2	750	366.2	505.2	37.8	69.3
3	800	342.2	501.4	36.2	67.0
4	850	400.3	513.7	33.0	64.2
5	900	354.3	505.0	37.3	63.9
6	950	358.9	502.4	37.2	68.4
7	1000	360.1	502.8	37.9	67.3
8		362.5	513.6	34.5	62.5
9		370.2	511.9	37.2	65.7
10		403.9	501.3	32.4	60.0
11		437.0	525.0	25.4	64.0

TABLE 4.5 Vickers hardness numbers.

SAMPLE NO.	HEAT TREATMENT TEMPERATURE (°C)	VICKERS HARDNESS NUMBER (HV ^{0.05})
1	700	170
2	750	163
3	800	168
4	850	172
5	900	165
6	950	171
7	1000	170
8	1050	167
9	1100	191
10	1200	185
11	1300	190

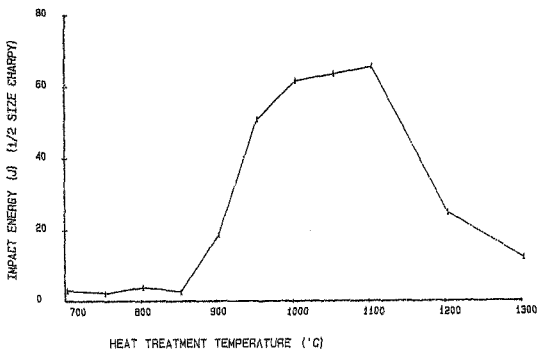


Figure 4.4 Impact energy versus heat treatment temperature.

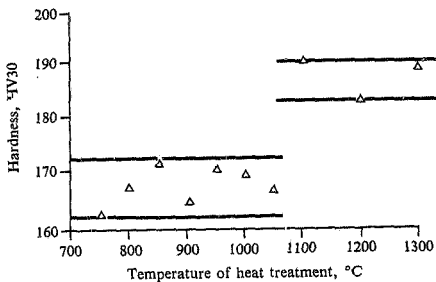


Figure 4.5 Hardness versus heat treatment temperature.

TABLE 4.6 DBTT values as determined from slow bend curves.

SAMPLE NO.	HEAT TREATMENT TEMPERATURE (°C)	DBTT (°C)
1	700	> 32
2	750	> 32
3	800	> 32
4	850	> 32
5	900	30
6	950	30
7	1000	22
8	1050	- 35
9	1100	- 25
10	1200	- 15
11	1300	17

The total area under the load-deflection curve was plotted against the test temperature in order to obtain slow-bend DBTT curves (Figure 4.6 (a) to (f)). Due to the scatter in the results, in several cases the fracture appearance was used to assist in drawing the curve. (In these cases, the percentages of ductile fracture have been included on the figures). The inconsistencies in both the slow-bend test results and the fracture appearance are evident for Sample 9. (Figure 4.6d). As noted with the impact energies, large deviations from average values were normally due to the presence of a flaw in the material. Although a slow-bend DBTT curve has been drawn from the information available, the accuracy is questionable.

The six DBTT curves are for the heat-treatments above 900 °C: 950, 1000, 1050, 1100, 1200 and 1300 °C. The samples heat-treated up to 900 °C for one hour had transition temperatures above ambient temperatures, and DBTT curves were not obtained for these σ -phase embrittled samples.

Figure 4.7 illustrates several methods available for calculating the ductile-to-brittle transition temperature from slow bend test data. The curves are for the samples heat-treated at 1050 °C. DBTT analysis is shown for:

1. the total area under the load-deflection curve versus test temperature;
2. the area under the curve to maximum load as a function of temperature;
3. the extent of the rapid load drop (corresponding to the onset of brittle fracture) as a function of test temperature; and
4. the fracture appearance transition temperature (FATT). Curve number 3 is plotted as the percentage of ductile fracture.

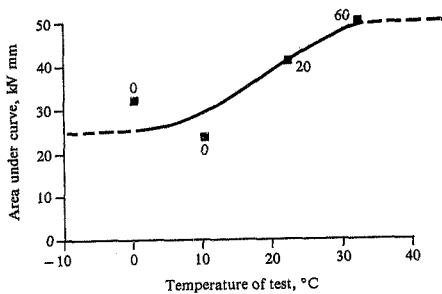
This is calculated using the equation:

$$\frac{\text{Max} - \text{drop}}{\text{Max}} = \% \text{ ductile fracture} \quad \dots (4.1)$$

where Max = the height of the slow bend curve measured at the maximum point; and

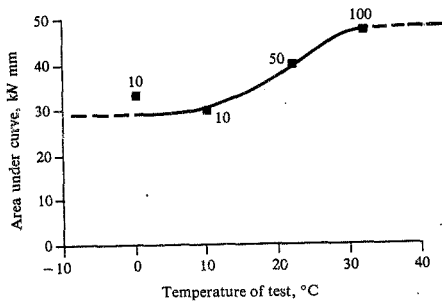
drop = the length of the rapid load drop measured on the slow-bend curve.

It can be seen that all the curves gave a DBTT of approximately -35°C .

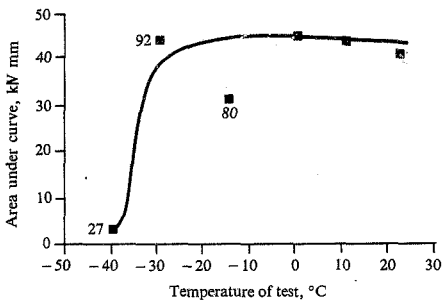


a) Slow bend sample 6 (950 °C)

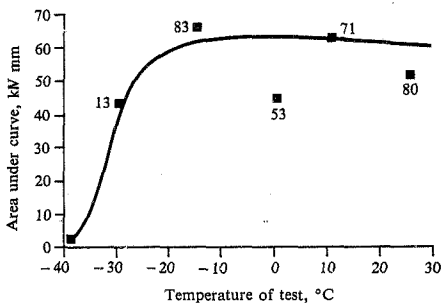
Figure 4.6 Slow-bend DBTT curves for Fe-40%Cr.



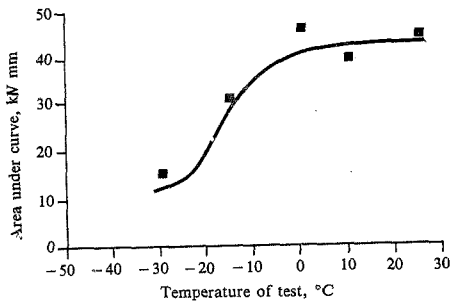
b) Slow bend sample 7 (1000 °C)



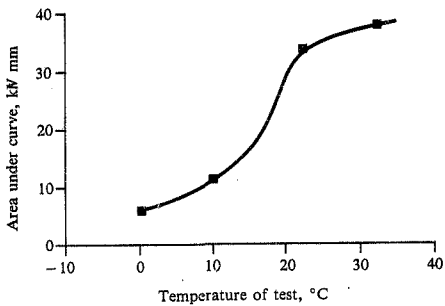
c) Slow bend sample B (1050 °C)



d) Slow bend sample 9 (1100 °C)



e) Slow bend sample 10 (1200 °C)



f) Slow bend sample 11 (1300 °C)

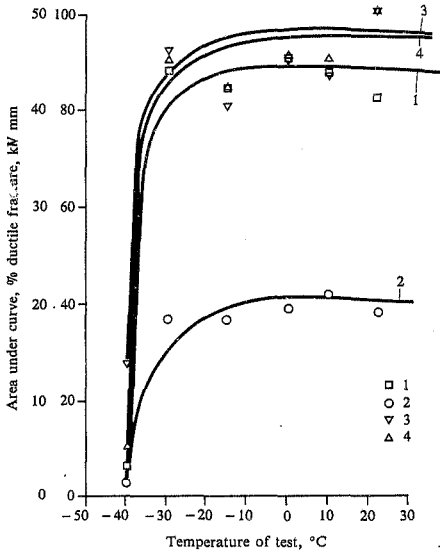


Figure 4.7 DBTT Analysis: Sample 8 (1050 °C).
 1=Full area 2=Area to max. point 3=% rapid drop
 4=Fatt.

4.3 Deformation and Fracture Mechanisms:

4.3.1 Slow-bend and Charpy V-notch specimens.

Observation of both polished and fracture surfaces yielded information regarding the deformation and fracture mechanisms in operation during Charpy impact tests and slow-bend tests for the various heat treatments studied. Table 4.7 summarizes the deformation and fracture mechanisms as a function of test type, test temperature and prior heat treatment. Several general observations may be made.

The σ -phase embrittled samples (i.e. 700 to 850 °C heat treatment) exhibited very little stress relief and a low energy brittle fracture for all test temperatures.

Figure 4.8 shows the fracture surface of a sample heat-treated at 700 °C and tested in slow-bend at ambient temperatures. The fracture occurred primarily by cleavage, although grain boundary separation can also be seen and there are small areas of void coalescence.

For samples with little or no σ -phase present, (i.e. samples heat-treated from 900 to 1100 °C) a general trend was observed. For samples tested in slow-bend above the DBTT, there was a high density of stress-relieving slip, extending into the sample. The fractures occurred by a combination of void coalescence and transgranular cleavage. The fraction of each fracture mode was a function of the test temperature and the related DBTT. There was a sharp transition from ductile-to-brittle fracture (Figure 4.9), although samples tested near the DBTT exhibited a "mixed" fracture. Voids formed along some grain boundaries within the brittle regions. (Figure 4.10).

TABLE 4.7 Observed deformation and fracture mechanisms of slow-bend and Charpy impact specimens following different heat treatments.

HEAT TREATMENT TEMP. (°C)	TEST TEMP. AND METHOD	DEFORMATION MECHANISMS	FRACTURE APPEARANCE
700 to 850 °C	32 °C and below slow-bend	A low density of slip bands adjacent to the fracture surface. No lateral expansion.	100% brittle cleavage and grain boundary separation. A small number of voids.
	22 °C Charpy impact	A low density of slip bands and twins adjacent to the fracture surface. No lateral expansion.	As above
900 to 950 °C	32 °C slow-bend	Slip bands extending ~5mm into sample	~60% ductile
	0 °C slow-bend	A small amount of lateral expansion. A high density of slip bands extending into sample.	100% brittle
	22 °C Charpy impact	Slip and twins corresponding to % brittle fracture. Slip and twins extending into sample	75% brittle
1000 °C	32 °C slow-bend	A few twins	100% brittle
	32 °C slow-bend	A high density of slip	100% ductile
	22 °C slow-bend	A high density of slip related to ductile fracture. Grains with very little slip related to brittle fracture	50% ductile
	10 to 0 °C slow-bend	A high density of slip	90% brittle
	22 °C Charpy impact	Predominantly twins	90 to 100% brittle

TABLE 4.7 (continued)

HEAT TREATMENT TEMP. ($^{\circ}$ C)	TEST TEMP. AND METHOD	DEFORMATION MECHANISMS	FRACTURE APPEARANCE
800 $^{\circ}$ C 1 hr plus 1000 $^{\circ}$ C 1 hr	22 $^{\circ}$ C Charpy impact	Slip and twins	100% ductile
1050 and 1100 $^{\circ}$ C	22 to -30 $^{\circ}$ C slow-bend	A high density of slip bands extending into the sample	100 to 10% ductile
1050 $^{\circ}$ C	-40 to -45 $^{\circ}$ C slow-bend	A few twins and slip bands near the fracture surface	90 to 100% brittle
1050 and 1100 $^{\circ}$ C	22 $^{\circ}$ C Charpy impact	Predominantly twins but some slip bands	100% ductile
1200 $^{\circ}$ C	32 to -15 $^{\circ}$ C slow-bend	Slip and twins	Very incon- sistent fracture appearance with temp- erature
	22 $^{\circ}$ C Charpy impact	Predominantly twins but some slip	20 to 100% brittle inconsistent fracture appearance
1300 $^{\circ}$ C	22 to 0 $^{\circ}$ C slow-bend	Predominantly twins but some slip	Inconsistent fracture appearance Large cleav- age facets with areas of ductility within
	22 $^{\circ}$ C Charpy impact	Predominantly twins	As for the slow-bend samples



Figure 4.8 Fracture surface of a slow-bend specimen from Sample 1 (heat-treated at 700°C) tested at ambient temperatures.



Figure 4.9 Fracture surface of a slow-bend specimen (Sample B) showing sharp transition from ductile to brittle fracture.

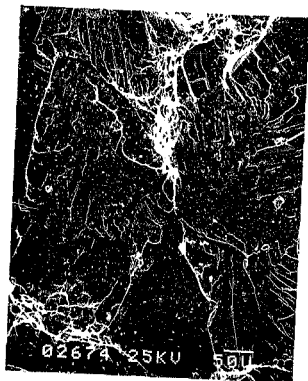


Figure 4.10 Fracture surface of Sample 8 tested in slow-bend near the DBTT (-40°C) showing a "mixed" fracture.

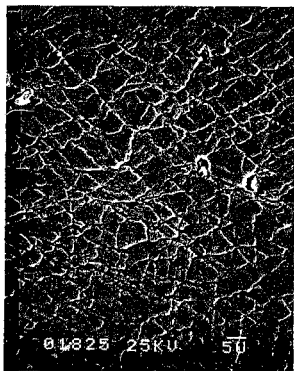


Figure 4.11 Deformation surface of slow-bend Sample 8 tested at -45°C , immediately adjacent to the fracture surface.

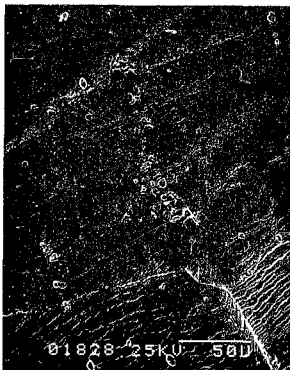


Figure 4.12 Deformation surface of slow-bend Sample 8 tested at -45°C , several grains from the fracture surface. (adjacent to the area of Figure 4.11).

As the test temperature decreased towards the DBTT for the slow-bend samples, the density of slip bands, and the distance they extended into the sample, decreased, and twinning was also observed. Below the transition temperature, deformation was very localized. Figures 4.11 and 4.12 are SEM photomicrographs of the deformation surface of the sample heat-treated at 1050 °C and tested at -45 °C. Immediately adjacent to the fracture surface (Figure 4.11) stress-relieving slip may be seen. Within a distance of only several grains of the fracture surface, however, there was no evidence of stress-relief (Figure 4.12) and microcracking could be seen associated with precipitates.

Samples fractured in a Charpy impact test, exhibited a predominance of twinning, the density of which related directly to the percentage of brittle fracture (i.e. less twinning for a more brittle fracture). A small amount of stress-relieving slip was also observed for samples exhibiting some ductility.

Regardless of the fracture mode or test temperature, a separation of the precipitate-matrix interface occurred within the region of deformation (see Figure 4.11), and cracking of precipitates was not observed.

The samples heat-treated at 1200 and 1300 °C had fracture surfaces which were very inconsistent with the test temperature. This was a result of the mixed grain size. Very large transgranular cleavage facets were observed, but there were areas of ductility between the facets. There was no sharp transition from ductile to brittle fracture. The predominant mode of deformation was twinning, although some stress-relieving slip was also observed.

4.3.2 Tensile Test Samples.

For the heat treatments up to and including 1100 °C the tensile test samples exhibited a ductile fracture surface. Although these specimens were not polished, a large amount of deformation was seen

along the length of the samples. Each grain within the deformation zone was distinguishable in a manner similar to that observed for the ductile slow-bend samples which exhibited a high density of slip bands.

The tensile test samples from material heat-treated at 1200 and 1300 °C exhibited a predominantly ductile fracture, with one or two large cleavage facets each. The degree of deformation was less for these samples than for the lower temperature heat-treatments.

4.4 Alloyed Fe-40%Cr

DBTT's of the modified Fe-40%Cr compositions were determined from Charpy impact tests over a range of temperatures. The results are listed in Table 4.8.

The upper shelf energies of the alloys are listed as > 360J, as this was the limit of the impact tester. The results of the room temperature tensile tests, and Vickers hardness tests are listed in Table 4.9.

No σ -phase was found in any of the alloys subsequent to heat treatment.

Table 4.3 DBTT and upper shelf energies for alloyed Fe-40%Cr determined from Charpy impact tests

Ingot	Alloy Analysis (Wt.%)	Alloy Addition (Wt.%)	DBTT (°C)	Upper Shelf Energy (J)
A	-	base alloy	50	140
B	0.2C	0.2 Nb	~ 90	-
C	0.07 Ti	0.2 Ti	> 90	-
D	0.12 Al	0.2 Al	- 10	> 360
E	0.19 Ru	0.2 Ru	40	125
F	0.03 Ti + 0.20 Ru	0.1 Ti + 0.2 Ru	0	170
G	2.0 Ni	2.0 Ni	- 25	150
H	< 0.02 Ti + 0.19 Ru	0.05 Ti + 0.2 Ru	- 15	330
I	< 0.02 Ti	0.05 Ti	- 15	330
J	0.1 Nb	0.1 Nb	10	200
K	< 0.02 Al + 0.09 Nb	0.2 Al + 0.1 Nb	0	> 360
L	0.98 Ni	1.0 Ni	- 5	185
M	< 0.02 Al + 2.00 Ni	0.2 Al + 2.0 Ni	- 18	360
N	0.17 Ru + 2.02 Ni	0.2 Ru + 2.0 Ni	- 10	180

Table 4.9 Results of hardness tests and ambient temperature tensile tests for alloyed Fe-40%Cr

Heat	Alloy Addition (wt.%)	Hardness (HV30)	% El	% R of A	Yield Stress (MPa)	UTS (MPa)
A	-	172	30.0	47.2	350.1	502.0
B	0.20 Nb	180	17.9	17.6	393.6	528.8
C	0.20 Ti	177	10.7	8.1	365.0	490.0
D	0.20 Al	174	32.2	57.6	345.2	494.4
E	0.20 Ru	175	25.3	44.5	360.0	497.0
F	0.10 Ti + 1.20 Ru	185	27.5	58.8	412.5	502.6
G	2.0 Ti	200	25.2	41.4	461.6	564.6
H	0.05 Ti	172	25.4	62.3	418.0	504.9
I	0.2 Ru + 0.05 Ti	179	22.6	54.9	399.4	499.6
J	0.1 Nb	178	24.6	58.3	411.0	502.9
K	0.2 Al + 0.1 Nb	179	25.0	68.6	402.5	512.0
L	1.0 Ni	182	19.9	56.9	448.7	531.1
M	0.2 Al + 2.0 Ni	194	20.8	65.2	484.0	570.6
N	0.2 Ru + 2.0 Ni	192	22.5	58.4	494.2	566.1

5. DISCUSSION

5.1 Introduction

Hochmann³ and Binder and Spendelow⁴ first showed that ferritic chromium steels could be rendered ductile at ambient temperatures by reducing the carbon and nitrogen contents. A large number of experiments have been carried out at MINTEK and the University of the Witwatersrand to determine a suitable melting procedure to obtain sufficiently high purity in Fe-40%Cr alloys. This has resulted in the routine obtainment of average carbon and nitrogen values of 0.006 and 0.005% respectively, ((C+N) = 110 p.p.m.), and average oxygen contents of 0.09%. These values remained constant throughout experimentation, prior to the addition of alloying elements.

Thermomechanical processing was used to refine the grain size and to increase the mobile dislocation density. The processed material was then subjected to one hour heat treatments at temperatures ranging from 700 to 1300 °C followed by a water-quench. The heat-treated material may be separated into three types:

1. σ -phase embrittled material;
2. "tough" material; and
3. high temperature embrittled material.

Alloying elements were added to the base Fe-40%Cr material in order to stabilize, deoxidize or "ductilize" the material. The additions were made as an attempt to counter the deleterious effects of the interstitial elements.

5.2 Rolling Parameters.

Preliminary experimentation was carried out in order to determine the optimum rolling parameters for this high-chromium ferritic alloy. The parameters investigated included soaking temperature (i.e.

rolling start temperature), initial soaking time, soaking time between each rolling sequence, and final rolling temperature.

According to the model of Ashby and Embury²¹, toughness increases as the grain size decreases and the number of mobile dislocations increases. Both of these requirements were achieved by ensuring that the final rolling temperature remained within the warm working regime.

When considering rolling and heat-treatment parameters, several factors had to be considered. The 400 to 550 °C temperature range had to be avoided in order to prevent 475 °C embrittlement. The σ -phase region also had to be avoided for long soaking times. Finally the soaking temperature had to be low enough to avoid rapid grain growth, yet high enough to dissolve any σ -phase that may have formed during rolling.

Figure 5.1 shows an SEM photomicrograph of an ingot after rolling between 750 and 600 °C. The σ -phase which formed was not dissolved in this temperature range. The presence of a large amount of this brittle phase resulted in large cracks, which caused the ingot to fracture into two pieces during rolling.

A soaking temperature and a rolling start temperature of 950 °C was chosen, as this was believed to be above the σ -phase formation temperature for this alloy, yet was low enough to avoid rapid grain growth. A minimum finish rolling temperature of 650 °C was used in order to prevent 475 °C embrittlement. This temperature was also found to be below the recrystallization temperature for this alloy, thus producing material in the warm worked condition. Using a thermocouple placed within a hole drilled in an ingot, it was determined that an initial one hour soak and 20 minutes between each rolling sequence was sufficient to obtain a homogeneous temperature of 950 °C.

Due to the high chromium content of this alloy, and the warm work introduced into the material, the kinetics of σ -phase formation



Figure 5.1 SEM photomicrograph showing cracking of σ -phase during rolling from 750 to 600 °C.

were increased. Thus, there was the possibility that σ -phase could form during rolling, since the final rolling temperature was within the temperature range for σ -phase formation. However, if σ -phase did form, the amount would be expected to be small. Thus, the soaking times and temperature were selected to ensure the dissolution of the σ -phase.

Experiments were also carried out for soaking temperatures of 1050 and 1150 °C. An optimum soaking temperature appears to be in the 950 to 1050 °C range. A soaking temperature of 1150 °C resulted in a

loss of toughness due to grain growth, although the annealing out of the mobile dislocations introduced during rolling could be a contributory factor. In the latter case, cracks which form may grow without capturing any dislocations.

5.3 σ -Phase Embrittled Material.

The presence of σ -phase was found in this Fe-40%Cr ferritic alloy after one hour heat treatments in the temperature range 700 to 900 °C. The σ -phase embrittled material exhibited ductile-to-brittle transition temperatures well above ambient temperature. The impact energies at ambient temperature were negligible. The fracture surfaces of the Charpy impact specimens and of the specimens broken in the slow-bend mode were similar. A typical fracture surface for the σ -phase embrittled samples was shown in Figure 4.8. Cleavage was the primary mode of fracture although grain boundary decohesion was evident and voids had formed at several precipitates then coalesced. No lateral expansion occurred for these fractured specimens.

Sigma-phase was found to form on grain boundaries and around precipitates. According to the theory of Tetelman and McEvily¹⁴, this embrittled material may be defined as a dirty material due to the inhomogeneous distribution of a brittle phase. Thus, the ease of slip-or twin-nucleated cleavage fracture will be increased. A low density of slip bands and twins was observed on the polished surface of the Charpy and slow-bend fractured samples immediately adjacent to the fracture surface. The deformation did not extend into the sample. There was thus very little stress-relief in this material. The large stress concentration which is set up at the tip of a slip band or twin will not be relaxed by plastic deformation when the brittle σ -phase is encountered, and therefore a cleavage crack may form. Cracks can be seen to be initiating at the grain boundaries and at the precipitates of a σ -phase embrittled sample (Figure 5.2). Very little stress-relieving slip was occurring. In the same photomicrograph, it can be seen that voids have formed around the precipitates. The fracture surface of Figure 4.8 also showed small

areas void coalescence resulting from the separation of the precipitate-matrix interface.

McMahon and Cohen¹⁶ hypothesized on the formation of a cleavage microcrack in ferrite. They stated that a crack initiates in a brittle precipitate and propagates across the precipitate as a Griffith crack. Throughout the present study no cracked precipitates (carbides, nitrides or oxides) were observed. However, cracking of the brittle intermetallic σ -phase was observed. (Figure 5.1). Thus, if the surrounding ferrite matrix is unable to yield due to a lack of stress-relieving slip, the matrix will accept the crack as a Griffith flow, and cleavage fracture may ensue. In addition the grain boundary decohesion which occurred in these σ -embrittled samples also produced crack-like defects, which could initiate fracture. (Figure 5.3).

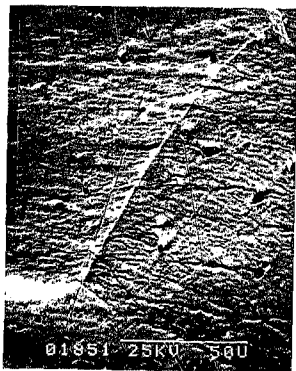


Figure 5.2 SEM photomicrograph of a slow-bend deformation surface for σ -embrittled Sample 1 (700 °C).



Figure 5.3 Fracture surface of a σ -embrittled specimen (Sample 1) showing grain boundary decohesion, and a twin intercepting a grain boundary.

A twin can be seen intercepting the grain boundary. The large stress-concentration at the tip of the twins as it encountered the brittle grain boundary phase, was the probable cause of decohesion.

The rhenium ductilizing effect appears to be related to the formation of σ -phase. Stephens and Klopp⁴⁹ found a minimum DBTT for the chromium-iron system when the alloy composition approached the σ composition, and when the alloys were quenched from the single phase region. Thus, they recognised the detriment of quenching these high-chromium alloys from the two-phase ($\alpha + \sigma$) region.

The tensile test samples for the specimens heat-treated in the range 700 to 900 °C exhibited ductile fractures. The elongation and reduction of area were in the same range (30 to 38% and 64 to 69% respectively) as the material classified as "tough" in this study (see Section 5.4). The ductility exhibited by the tensile samples was probably the result of the low strain rate ($3.3 \times 10^{-2} \text{mm S}^{-1}$) and the uniaxial nature of the tension. The yield stress in bcc metals is very sensitive to both temperature and strain rate, and a ductile-to-brittle transition occurs for these metals as the temperature is decreased, or the strain rate is increased.⁶ Thus, with a lower uniaxial strain rate, slip bands or twins form more slowly, and there is time for relaxation to occur at the brittle phase. The work done in crack nucleation will increase with the decrease in strain rate. The absence of a stress-raising notch in the tensile samples will also tend to increase the ductility. Superior results would be expected therefore from this sample configuration as compared to the notched slow-bend samples which were tested in tri-axial tension.

The yield stress does not vary linearly with heat treatment temperature in the 700 to 900 °C range. (Figure 4.3) This is probably due to the presence of σ -phase which resulted in a large variation in the mechanical properties. However, one point which may be noted from the curve of Figure 4.3 is that the maximum yield stress for this temperature range occurred at 850 °C. This coincides with the predicted nose of the σ -phase formation curve.

Transmission electron microscopy revealed the presence of a high density of dislocations in samples containing σ -phase. At 700 °C, most of these dislocations had rearranged to form sub-boundaries by the process of recovery. (Figure 5.4) The formation of the brittle intermetallic phase at grain boundaries and precipitates will produce localised stresses and serve to increase the dislocation density. Nevertheless, this appears unable to provide sufficient stress-relief to prevent the cracking of the brittle σ -phase.

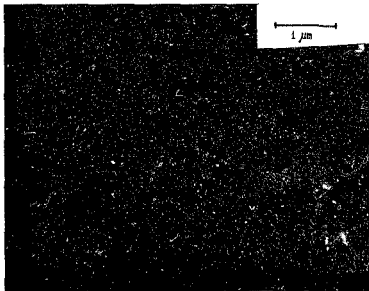


Figure 5.4 TEM photomicrograph of Sample 1 (heat-treated at 800 °C) showing recovery of dislocations.

5.4 "Tough" Material.

Samples of Fe-40%Cr which had been heat-treated between 950 and 1100 °C exhibited ductile-to-brittle transition temperatures below ambient temperature. A minimum slow-bend DBTT of -35 °C was obtained for this alloy after a one hour heat-treatment at 1050 °C. The ambient temperature impact energies, obtained from half size Charpy samples ranged from 50 to 65 J. The DBTT values calculated from the slow-bend curves gave similar results to the fracture appearance

transition temperatures (FATT). The fractured samples showed a transition from a high energy ductile fracture to a low energy brittle fracture. The sharp transition from ductile-to-brittle fracture in this ferritic alloy (as illustrated in Figure 4.9) may be explained using the Cottrell equation.

$$\sigma_y \propto k_y d^{1/2} \propto B \mu \gamma \quad \dots (2.2)$$

The yield stress in bcc metals is sensitive to temperature as well as to strain rate. As a fibrous crack progresses through the material, the strain rate at the tip of the crack will increase resulting in an increase in σ_y . As the strain rate at the tip of the crack increases, the time available for relaxation to occur as the crack encounters a barrier decreases. Thus, the number of dislocations released into a slip band will also decrease, resulting in an increase in k_y , the Hall-Petch slope. In addition, the stress concentration will effectively lower the surface energy γ of the material. The Cottrell equation will be satisfied at some point as a fibrous crack progresses, and a cleavage crack will then form ahead of the fibrous crack.

Samples which were tested above their DBTT exhibited fracture primarily by void coalescence, although small areas of cleavage fracture often occurred within the ductile regions (Figure 5.5). In all instances, these areas were associated with large (10 to 15 μ m) precipitates. Very little stress relaxation would occur as a slip band or twin was blocked by these large precipitates, and a cleavage crack would form. However, conditions in the matrix remained such that the cleavage crack would be quickly blunted and the crack would continue to propagate in a fibrous mode.

At temperatures below the DBTT, the primary mode of fracture was transgranular cleavage, although void coalescence did occur in small areas. The fact that there was always a separation of the particle-matrix interface rather than cracking of the precipitates is indicative of stress relaxation occurring around the precipitates.

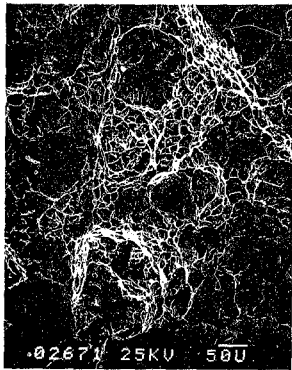


Figure 5.5 Fracture surface of Sample 8 fractured above the DBTT (10 °C). Areas of cleavage are associated with large precipitates within the ductile fracture.

The rolling schedule of this material was such that the final rolling temperature was in the σ -phase formation range. During rolling σ -phase was found to form on the grain boundaries and around precipitates. (see Figure 4.1) This would result in an increased dislocation density at the $\sigma - \alpha$ interface. The one hour heat-treatments above 900 °C were found to dissolve the σ -phase. Using electron microscopy (Figure 5.6) it was found that subsequent to dissolution of the σ -phase, a high density of dislocations remained at the grain boundaries and associated with other precipitates.

Samples which had been heat-treated in the temperature range from 950 to 1100 °C exhibited little variation in the yield stress. (see Figure 4.3) The lack of sensitivity of the yield stress to the annealing temperature in this temperature range may be indicative of the occurrence of a phenomenon such as the rhenium ductilizing effect. When rhenium and its analogues, such as iron, are added to chromium, both the temperature and the strain rate sensitivity of the yield stress decrease.⁴⁸

In the present study, it was found that a one hour anneal in this temperature range was sufficient to dissolve the σ -phase which had formed during rolling. It is proposed that the localized stresses, which formed in the material as a result of σ -phase formation, act as sources for the generation of dislocations. These are retained during annealing and result in increased toughness, and a reduction in the DBTT.

A general trend in the deformation mechanisms was observed for the "tough" material. (This reference to "tough" material relates to material with a slow-bend DBTT below ambient temperatures.) Above the DBTT, the high density of stress-relieving slip is again probably the result of the formation and dissolution of σ -phase as suggested above. Figure 5.7 shows a high density of wavy slip bands encountering a grain boundary. There is no evidence of microcracking in contrast to σ -phase embrittled samples (see Figure 5.2). Rather, the stress concentration is able to be relaxed due to the high dislocation density which is present.

As the DBTT was approached, the density of the slip bands decreased, and the distance which they extended away from the fractured surface of the slow-bend specimens also decreased.

Below the DBTT, twinning became the predominant mode of deformation, although some slip bands were still present.

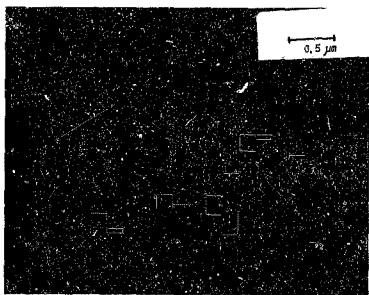


Figure 5.6 TEM photomicrograph of Sample 8 (1050 °C). A high dislocation density is present at the grain boundaries and precipitates.

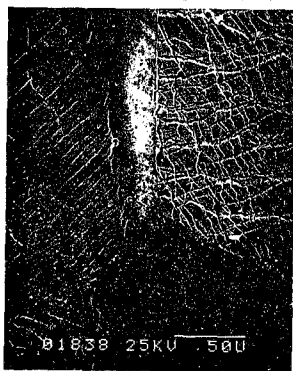


Figure 5.7 Slip bands encountering grain boundaries of Sample 8 (1050 °C).

The Peierls-Nabarro stress increases with a decrease in temperature as a result of the reduction in the thermal enhancement of the dislocation mobility, and the slip band density is consequently reduced. Figure 5.8 is a photomicrograph of the deformation surface of a sample which had been annealed at 1050 °C and fractured in slow-bend at -45 °C (i.e. below the DBTT).

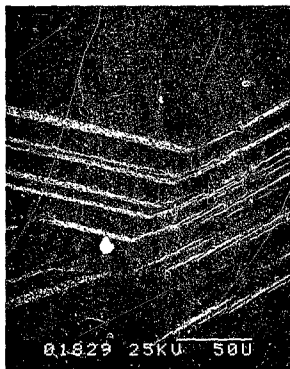


Figure 5.8 Deformation surface of Sample 8 fractured in slow-bend below the DBTT (-45 °C). Microcracking is occurring at the tips of twins.

Relaxation is not occurring, but rather the stress concentration at the tip of twins has caused microcracking to occur at a barrier such as a grain boundary.

The predominance of twinning as the test temperature decreased agrees with theory. At lower temperatures, the stress required for slip to occur increases, while that for twinning remains essentially unchanged, and twinning becomes the preferred mode of deformation.¹⁴

Twinning was also found to be the primary mode of deformation in the Charpy impact specimens. This was due to an increase in the strain rate rather than a decrease in the test temperature, which indicates that the stress required for slip is both temperature and strain-rate controlled. At higher strain-rates, twinning appears to be the preferred mode of deformation. This is supported by the results of the low strain rate tensile tests in which a significant amount of deformation and a ductile fracture mode were observed.

In some instances, Charpy V-notch impact energies were obtained which deviated greatly from the average value for a specific heat treatment. These deviations were listed in Table 4.3 as a second impact energy value. These large deviations were invariably found to be related to the presence of flaws or large non-metallic inclusions in the material. Very little stress relaxation can occur when a slip band or twin encounters such large flaws at these high strain-rates, thus a cleavage crack will progress easily through the material.

The variation in toughness for slow-bend and tensile test samples was much less extensive. Sample 9 exhibited the greatest inconsistencies for slow-bend test results, and therefore an accurate DBTT could not be obtained. The inconsistencies are believed again to be the result of casting flaws in the ingot.

Due to the lower strain-rates of slow-bend and tensile tests, there is some time for relaxation to occur which is possibly sufficient for the activation of slip band and twin sources around the flaw. Thus,

the presence of a flaw or large non-metallic inclusions is very detrimental to the impact properties of this ferritic alloy, but this detriment is decreased if fracture occurs at a lower strain rate.

To further investigate the formation and subsequent dissolution of σ -phase as a "ductilizing" method for these high chromium ferritic alloys, a series of tests were carried out. Charpy V-notch test specimens which had been annealed for one hour at 800 or 850 °C followed by a water quench were known to be σ -phase embrittled. These samples were annealed for one hour at 1000, 1050 and 1100 °C followed by a water quench. The impact energies for these samples were higher than those which had been annealed at the same temperatures following rolling. (i.e. without the intermediate anneal in the σ -phase formation range). A larger amount of σ -phase will be formed during the one hour anneal at 800 or 850 °C as compared with the amount present subsequent to rolling to a minimum temperature of 650 °C. The greater the amount of σ -phase which is formed, the greater will be the resultant dislocation density generated at the α - σ interfaces. Subsequent to dissolution of the σ -phase in the temperature range of 1000 to 1100 °C, a larger number of mobile dislocations will remain to allow relaxation of concentrated stresses as slip bands or twins are blocked by barriers such as grain boundaries or precipitates.

Although the formation of larger amounts of σ -phase appears beneficial, considerable care must be taken during processing. If this phase becomes cracked, it will severely embrittle this flaw-sensitive material. In this case, subsequent dissolution will not enhance toughness.

5.5 High-Temperature Embrittled Material

The volume percent of precipitates present in this high chromium alloy subsequent to heat-treatments up to 1050 °C was found to remain fairly constant in the 1% range. (Figure 4.2) This value decreased to the 0.6% range following heat-treatments at 1100 to 1300 °C. It may be hypothesized that above 1050 °C, the carbon and nitrogen were

in solution. Although this could not be verified on the microprobe due to the small amounts of carbon and nitrogen present in these alloys, support for this assumption was gained from transmission electron microscopy. Figure 5.9 shows an electron micrograph of the sample quenched from 1300 °C.

Many small precipitates can be seen within the grains, and pinning of the dislocations is also occurring. Dislocation loops, which are present in this sample, were not observed in lower temperature annealed samples, therefore they are probably not a quenching effect. Rather, they probably arose to relieve the misfit due to differential thermal contraction between the precipitates and the matrix.

These precipitates could not be seen optically, and are beyond the resolution of the image analyser. Thus the drop in observable volume percent precipitates appears to be due to the phenomenon known as high temperature embrittlement. Demo³² observed the precipitation of chromium-rich carbides and nitrides on dislocations within the grain body, subsequent to quenching AISI Type 446 from 1100 °C. At these high temperatures, the carbon and nitrogen were in solution, and rapid precipitation occurred during quenching in order to relieve the supersaturation of interstitials. It was suggested that the effect of the rapid precipitation was similar to precipitation hardening.

The hardness of the present experimental alloys was found to increase from average values of 170 VHN to approximately 190 VHN for heat treatment temperatures up to, and above 1050 °C, respectively (Figure 4.5).

The slope in the yield stress versus heat treatment temperature curve, (Figure 4.3) was found to increase from 0.08 MPa/°C for heat-treatment temperatures of 900 to 1100 °C to 0.33 MPa/°C for those of 1100 to 1300 °C. This increase in yield stress may be explained using the Hall-Petch equation:

$$\sigma_y = \sigma_1 + k_y d^{-1/2} \quad \dots (2.1)$$

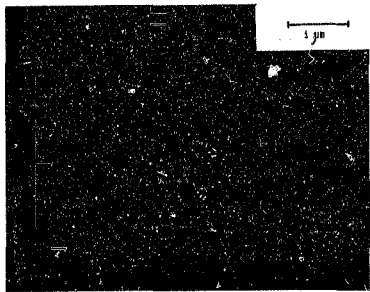


Figure 5.5 TEM photomicrograph of a sample quenched from 1300 °C. Small precipitates, dislocation pinning and dislocation loops can be seen within the grains.

The small precipitates will tend to lock the dislocations, resulting in an increase in σ_i , the lattice friction stress, and in k_y , which is a measure of the pinning of dislocations. A great variation in the grain size of samples heat-treated at 1200 and 1300 °C was found. However, the average size was larger than for lower temperature treatments, and several very large grains (with diameters greater than 300 μm) were observed in these samples. Since this increase in the grain size, d , would result in a decrease in the yield stress, this is further evidence for precipitation hardening. The effect of

dislocation locking on the yield stress appears to be greater than that of grain growth. In addition, the predominance of twinning as a mode of deformation increased for these samples quenched from high temperatures, and again this would be favoured by dislocation locking.

The impact energies decreased as the annealing temperature increased from 1100 to 1300 °C (Figure 4.4) due to both dislocation locking and the increase in grain size. The fracture appearance for both the *slow-bend* and the *Charpy* samples was very inconsistent for specimens annealed at 1200 and 1300 °C. In fact, it was not possible to determine a fracture-appearance-transition-temperature (FATT). This inconsistency was due to the heterogeneous grain size distribution in these samples. There was no sharp transition from ductile to brittle fracture, rather there were large cleavage facets within regions of ductile fracture.

In spite of all the evidence of dislocation locking, and high-temperature embrittlement, the DBTT values remained below ambient temperatures for these samples. High-temperature embrittlement has been claimed to be a phenomenon in only medium-to-high-interstitial ferritic alloys.^{15 22 32} The present evidence indicates that the precipitation of carbides and nitrides as a result of supersaturation was occurring as the alloys were quenched from the high temperatures. The present chromium content is greater than that in the alloys which have been previously studied to observe high-temperature embrittlement^{15 22 32} and the interstitial solubility has been shown to decrease with increasing chromium content.⁹ Thus the precipitation hardening observed in the present study would be expected at the lower interstitial levels.

The temperature at which the hardness, yield stress and DBTT began to increase, and the impact energy began to decrease for these Fe-40%Cr alloys, was 1100 °C.

It has been reported that high-temperature embrittlement occurs when ferritic alloys are quenched from above 1000 °C. All of these

studies have been carried out using ferritic alloys containing less than 30% chromium. The optimum toughness and ductility were found for this Fe-40%Cr alloy after a heat treatment at 1050 °C. The temperature of interstitial solution is thus believed to be above 1050 °C.

5.6 Alloyed Fe-40%Cr

The work on alloying of Fe-40%Cr to improve the low temperature ductility was carried out only as a preliminary investigation. From the literature available and also from the study of the unalloyed wrought material, several compositions were chosen for mechanical testing. The fabrication parameters for this series of alloys differed from those of the original investigation. The cast ingots were smaller in section due to a change in mould geometry, and the rolling reduction was decreased to provide full-size Charpy specimens. All of the alloys were then annealed for one hour at the proposed optimum temperature of 1050 °C.

Alloy A was a base Fe-40%Cr alloy used as a standard to compare the effects of the alloying additions. This material exhibited a CVN DBTT of 50 °C and an upper-shelf energy of 140 J. By comparing this alloy with Sample 8 of the original investigation, the effects of thermomechanical treatment can be assessed. Sample 8 exhibited a slow-bend DBTT of -35 °C after a one hour anneal at 1050 °C. It was reduced from an initial 45mm to a final thickness of 6mm (87%) whereas Alloy A was rolled from 38 to 12mm (68%). In the latter case there was less warm work put into the material. In addition this ingot contained less σ -phase since it was held for much shorter times in the critical temperature range during rolling. Due to the effects of a reduction in both the amount of work and σ -phase formation, a much lower density of stress-relieving mobile dislocations would be expected, as compared to Sample 8. This partially explains the increase in DBTT for Alloy A. (see Section 5.4). Secondly, the severity of the test to determine the DBTT's was different. The original ingots were tested using a 3-point slow-bend test, whereas Alloy A was tested using the Charpy V-notch impact test. The latter is known to be a more severe test due to the high strain rate and to

result in higher DBTT values. Finally, the size of the test samples must be considered. As shown by Nichol¹⁹, the DBTT is strongly influenced by gauge size. Thus again, inferior results would be expected from the full-size Charpy tests, compared with the smaller specimen geometry.

All of the considerations discussed above will also apply to the alloyed material (Alloys B to N).

Alloys B and C were stabilized with 0.2%Nb and 0.2%Ti respectively. The relevant stabilizer: (C+N) ratios added and recovered in the melt are listed in Table 5.1. (It is interesting to note that all of the niobium was recovered compared with only 35% of the titanium).

TABLE 5.1 The Stabilizer: (C+N) ratios added and recovered for Alloys B and C.

ALLOY	STABILIZER ADDITION: (wt %)	RATIO OF STAB:(C+N) ADDED		RATIO OF STAB:(C+N) RECOVERED	
		WEIGHT	STOICHIOMETRIC	WEIGHT	STOICHIOMETRIC
B	0.2 Nb	16	2	16	2
C	0.2 Ti	16	4	5.8	1.5

Both of these alloys exhibited ambient temperature brittleness with CVN DBTT's above 90 °C. It is well known that "over-stabilizing" embrittles these materials, and Wood²⁹ stated that titanium is a very potent solid solution strengthener. Grubb et al²⁷ showed that stabilization of Fe-26%Cr alloys with (C+N) levels under 100 p.p.m. was detrimental due to intergranular microcrack formation. As a result of the melting practice which has been established in this study, the combined carbon and nitrogen level in these alloys was approximately 120 p.p.m. Although this value is only slightly higher

than that proposed by Grubb et al, the tolerance for interstitials has been shown to decrease markedly with increasing chromium content⁹. Therefore, stabilization would be expected to be beneficial in this case. However, both the hardness and the yield stress of the stabilized alloys have increased above those values for standard Alloy A, as a result of solid solution strengthening and dislocation locking. This suggests that these alloys have been over-stabilized.

Two further alloys were made in order to study if lower levels of stabilizer could be beneficial at the carbon and nitrogen levels present. The addition of 0.05% Ti (Alloy H) and of 0.1%Nb (Alloy J) rendered this alloy ductile well below ambient temperature, and resulted in high upper shelf energies. In both cases these additions were just greater than the stoichiometric equivalent of (C+N).

Again, all the niobium was recovered and the results indicate that correct stabilization can be effective in providing good DBTT and toughness values.

The results for titanium stabilization appear anomalous. Although the stoichiometric equivalent of (C+N) was added, less than 0.02%Ti was recovered, yet this produced superior results to those of Alloy J (0.1%Nb). This is difficult to explain. One possibility is that it is not necessary to fix all the carbon and nitrogen, but merely to reduce it below a critical level. It has been suggested²⁷ that "overgettering" of carbon can be deleterious, since carbon in solution may reduce the embrittlement produced by oxygen which segregates at grain boundaries. In addition, higher quantities of precipitates may be more detrimental than low levels of carbon and nitrogen in solution, in terms of their influence on dislocation mobility. The possibility also exists that the titanium which is lost during melting may remove the interstitials into the slag, although the interstitial analysis does not support this proposal.

The results suggest that stabilization of these low interstitial-containing alloys can be beneficial provided that the correct level of stabilizing element is added.

Finally, the kinetics of σ -phase formation are known to increase due to the addition of titanium or niobium to ferritic alloys.^{26 35 45} The improved toughness of these stabilized alloys as compared with Alloy A is believed to be partially the result of the increased formation and dissolution of σ -phase and the subsequent increase in the mobile dislocation density.

The alloy containing 0.2%Al (Alloy D) was ductile down to -10 °C, with an upper shelf energy greater than 360 J. A total of 0.12%Al was detected in the final product and the oxygen content had been reduced to 0.029%. This oxygen level represents 25 to 50% of that normally obtained using the established method of melting. The aluminium has therefore served to deoxidize the material. The microprobe analyses reported in Section 4.1, indicated that the majority of the precipitates present in these experimental alloys were oxides of chromium. A decrease in the DBTT of Alloy D relative to the standard Alloy A reflects the dependence of the DBTT on the volume of second phase particles as cited by Plumtree and Gullberg¹³.

Most investigations into ferritic stainless steels state that desirable properties are achieved through the control of interstitial carbon and nitrogen. Little mention has been made of oxygen control and Wright²⁶ suggested that "preoccupation with oxide involvement in commercial ferritic stainless steel brittleness seems unwarranted." In the present alloys, the removal of oxygen has served to greatly improve their ductility.

Demo²⁴ suggested the use of aluminium as a "weld ductilizer" to control the interstitials (C+N) in high-chromium ferritic steels. The discrepancy found between the literature and the present experimental alloys may be due to variations in the C, N and O levels, although, generally the oxygen levels have not been quoted in the literature.

The combined effects of aluminium as a deoxidizer, and niobium as a stabilizer were tested in Alloy K. The resulting DBTT of 0 °C represents an improvement over the alloy which was only stabilized

(Alloy J). However, the DBTT was higher than that for the alloy which was only deoxidized (Alloy D) despite the presence of the lowest oxygen levels after the combined addition. This again may be due to over-stabilization.

The addition of 0.2%Ru (Alloy E) to Fe-40%Cr resulted in a 10 °C reduction in the DBTT (from 50 to 40 °C). Botli Demo²⁴ and Sipos et al³⁰ have suggested the use of other platinum group metals (P.G.M.'s), including platinum and palladium as "ductilizing additives". Although the reasons for ductility enhancement are not understood, Wright²⁶ suggested that they may entrap interstitials. The present results indicate that ruthenium may behave in a similar way as a "ductilizing additive".

The combined addition of 0.2%Ru and 0.1%Ti (Alloy F) gave a DBTT of 0 °C. Again the weight ratio of Ti: (C+N) recovered was only 2:1 compared with the quantity added which was 6.7:1. Nevertheless, the titanium does appear to be beneficial.

When the titanium addition was closer to the stoichiometric equivalent of (C+N) (Alloy I) the improvement due to the combined addition of Ru and Ti was even greater. This confirms that the correct level of stabilization is a very important factor in these low interstitial alloys. The DBTT and upper shelf energy for Alloy I were the same as those for Alloy H which had only the titanium addition. This suggests that if the alloy has been correctly stabilized, the effects of ruthenium as a "ductilizing additive" are neutralized. The entrapment of interstitials, as suggested by Wright²⁶, will not be necessary if they are precipitated.

The addition of 2.0%Ni (Alloy G) produced a DBTT of -25 °C. A smaller addition of 1.0%Ni (Alloy L) provided less improvement in ductility. The suppression of the CVN DBTT of high-chromium ferritics alloyed with nickel has been demonstrated previously⁵³. It has been suggested that the beneficial effect of nickel is related to its distortion of the ferrite lattice and the subsequent entrapment of interstitial solute.

Since the distortion will depend on the quantities added, this can explain the smaller effect of only 1%Ni on the DBTT. Additions of 0.2%Al (Alloy M) and 0.2%Ru (Alloy N) were made to the Fe-40%Cr-2%Ni alloy. In both cases, the DBTT was slightly raised above that for Alloy G (+2%Ni), and the toughness was increased.

The addition of nickel resulted in the greatest improvement in ductility (i.e. the lowest DBTT) for these ferritic alloys. The temperature sensitivity of bcc metals is known to be related to the (temperature-sensitive) Peierls-Nabarro stress.⁶ This stress depends on the width of a dislocation or the distance over which the lattice is distorted due to the dislocation. It is possible that the addition of an element which distorts the ferrite lattice decreases the Peierls stress and thereby decreases the temperature sensitivity of the metal. This would result in the lowering of the DBTT.

In all cases, the addition of 0.2%Al resulted in the greatest toughness in this Fe-40%Cr alloy with an upper-shelf energy of greater than 360 J (the limit of the impact equipment). The aluminium served to deoxidize the material, mainly through the removal of oxygen to the slag, and thus the number of second phase precipitates was reduced. Cleavage fracture has been shown to be dependent on the cleanliness of a material.¹⁴ The removal of second phase precipitates will therefore decrease the possibility for cleavage crack nucleation, which is the important step in the brittle fracture of ferritic steels.⁹

6. SUMMARY

The high toughness and low DBTT's which have been observed for this high chromium ferritic alloy subsequent to heat-treatments in the 950 to 1050 °C range appear to be due partially to a phenomenon known as the rhenium ductilizing effect.

To date, ferritic stainless steels have been found to have limited ductility and/or toughness at ambient temperatures. This inherent low temperature brittleness has been attributed to the fact in bcc metals that the yield stress is sensitive to changes in temperature and strain-rate as well as to the fact that bcc metals contain less mobile dislocations as compared to fcc metals.

In the present investigation, the ferritic alloys were rolled from a temperature above the σ -phase formation range, to a temperature below the recrystallization temperature and within the σ -phase formation range. This served the dual purpose of refining the grain size and allowing σ -phase to form at the grain boundaries and existing precipitates. An anneal above the σ -phase formation range (i.e. in the temperature range of 950 to 1050 °C) resulted in dissolution of the σ -phase. The mobile dislocations which had formed as a result of the localized stresses produced at the α - σ interface were found to remain. The effective result of the formation and dissolution of σ -phase in this bcc alloy was to increase the mobile dislocation density, decrease the temperature sensitivity of the yield stress and thereby reduce the ductile-to-brittle transition temperature to below ambient temperatures.

Heat-treatments below 950 °C resulted in σ -phase embrittled material, while those above 1050 °C showed indications of high-temperature embrittlement.

Proper stabilization of these low interstitial Fe-40%Cr alloys was found to be advantageous to the toughness and ductility. However the required amount of stabilizer was critical. The addition of

aluminum which served to deoxidize the material, resulted in the greatest toughness since the ease of cleavage crack nucleation was significantly reduced. The maximum improvement in ductility was obtained after the addition of 2%Ni. The nickel is believed to distort the lattice and thereby entrap the interstitials. It is also hypothesized that the nickel addition reduces the Peterls stress (due to the distortion of the lattice) and therefore decreases the temperature-sensitivity of the metal. Ruthenium appears to have a small beneficial effect on the ductility of this alloy. However its effects are negated in the presence of titanium or nickel additions.

7. CONCLUSIONS AND RECOMMENDATIONS FOR FURTHER WORK

7.1 Conclusions

1. The toughness of this ferritic alloy is related to the mobile dislocation density which may be increased by warm working the material and/or by the formation and dissolution of σ -phase at the grain boundaries and second-phase precipitates.
2. The increase in mobile dislocation density decreases the temperature and strain rate sensitivity of the yield stress, thereby increasing the toughness and reducing the DBTT.
3. Optimum properties may be obtained by soaking the alloy in the temperature range 950 to 1050 °C, rolling to a minimum temperature of 650 °C, and dissolving the σ -phase formed during rolling in the same temperature range.
4. Quenching of these alloys from above 1100 °C resulted in an increase in the hardness, the yield stress, the DBTT and the predominance of deformation by twinning, and a decrease in the impact energy. These factors are indicative of a phenomenon known as high temperature embrittlement, similar to precipitation hardening.
5. The addition of nickel to entrap the interstitials, aluminium to deoxidize the material and/or titanium or niobium to stabilize the material are all beneficial to the toughness and ductility of these alloys.

7.2 Recommendations For Further Work.

1. It is recommended that further work be carried out to determine whether the enhancement of properties due to the formation and dissolution of σ -phase to increase the mobile dislocation density could be achieved through heat-treatment of cast alloys rather than through thermomechanical treatment.

A suggested process would be to heat-treat the cast alloys within the α -phase formation range (eg. 800 to 850 °C) then to dissolve the α -phase at 950 to 1050 °C.

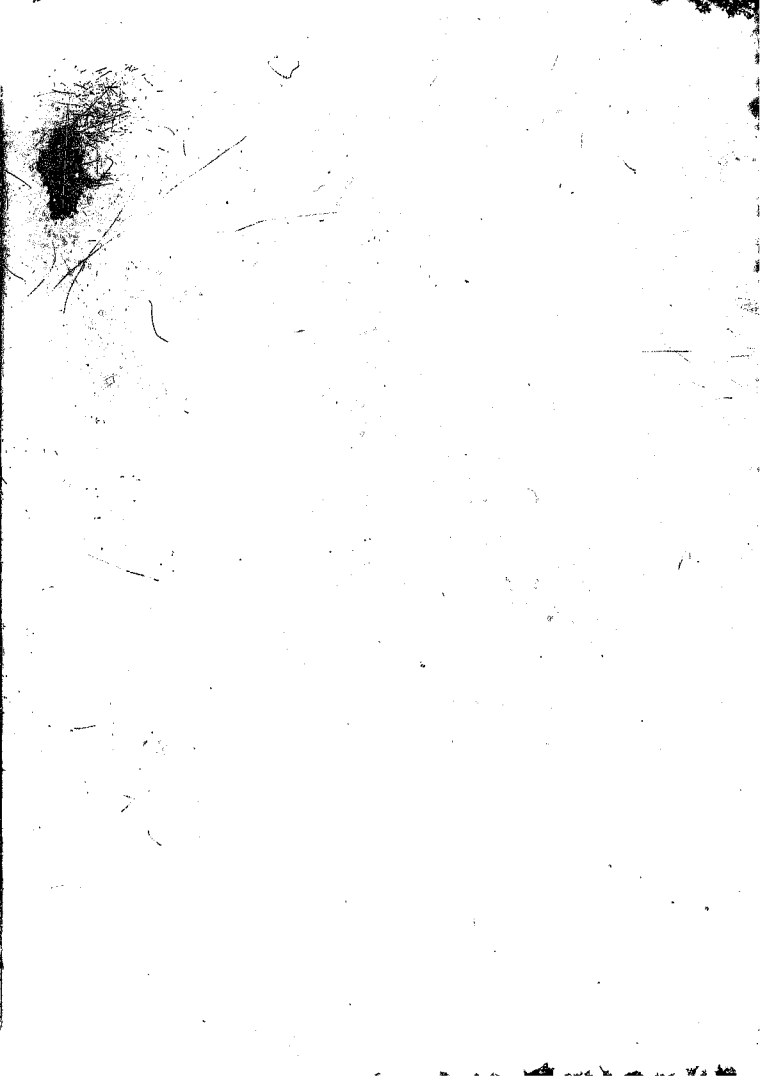
2. Further work should be done to examine the possibility of obtaining acceptable mechanical properties with higher levels of stabilized carbon and nitrogen present. The use of aluminium as a deoxidizer would still be necessary, however either less expensive starting materials or melting techniques could be possible.
3. It is necessary to ascertain the optimum addition of nickel with regard to both required ductility and cost.
4. Ruthenium appears to have a small ductilizing effect and is known to greatly improve the corrosion properties of these alloys. Further work should be done to determine the optimum alloying additions with ruthenium to obtain acceptable mechanical properties.
5. The use of other P.G.M. additions, such as platinum, as a ductilizer and corrosion resistance enhancer should be investigated.
6. All of the alloys of Fe-40%Cr were only tested for mechanical properties including toughness, ductility, strength and hardness. Further work such as fracture, deformation and microstructural analysis must be carried out in order to better understand the fundamental reasons for the changes in these properties as a result of the alloy additions. In this way, the optimum alloy additions could be determined.

8. REFERENCES

1. Tomashov, N.D. and Chernova, G.P. New corrosion-resistant alloys based on titanium and high-chromium steels. Protection of Metals, 11, 1975, pp.379-384.
2. Chernova, G.P. et al. Effects of alloying on the passivation of Fe-Cr based alloys. Corrosion, 34, 1978, pp.445-448.
3. Hochmann, J. Rev. Mét., 1951, 48, p.734.
4. Binder, W.O. and Spindelov, H.R. Trans. ASM, 1951, 43, p.759.
5. Rakitsky, A.N., Tkachenko, V.G. and Trefilov, V.I. Phys. Met. Metallorgr., 35, 1983, pp.82-88.
6. Hertzberg, R.W. Deformation and fracture mechanics of engineering materials. John Wiley and Sons, 1976.
7. Cottrell, A.H. The Properties of Materials at High Rates of Strain. Institute of Mechanical Engineering, London, 1957.
8. Gilbert, A., Reid, C.N., and Hahn, G.T. J. Inst. Met., 1963-1964, 92. pp.351-356.
9. Pillard, B. Welding Research Supplement, Apr. 1972, pp.222s-230s.
10. Hall, E.O. Proc. Phys. Soc., 1951, 3, p.22.
11. Petch, N.J. J. Iron Steel Inst., 1953, 173, p.25.
12. Cottrell, A.H. Trans. TMS-AIME, 212, 1958, pp.192-203.
13. Plumtree, A., and Gullberg, R. Influence of interstitial and some substitutional alloying elements. Toughness of ferritic stainless steels, ASTM STP 706, R.A. Luta, Ed., ASTM, 1980, pp.34-55.
14. Tetelman, A.S. and Mcevely, A.J., Jr. "Fracture of Structural Materials", 1967, John Wiley and Sons Inc., New York.
15. Grubb, John F. and Wright, Roger N. Inst Trans., 10A, Sep. 1979, pp.1247-1255.
16. McMahon, C.J., Jr. and Cohen, M. Acta Metallurgica, 13, 1965, pp.591-604.
17. Veistinen, M.K. and Lindroos, V.K. Application of fracture mechanics to materials and structures. Proc. Conf., Freiburg, FRG, 21 to 24 June, 1983, pp.377-391.
18. Reid, C.N. Met. Trans. A., 12A, March 1981, pp.371-377.

19. Nichol, T.J. Met. Trans., 8A, 1977, 9. 229.
20. Wright, R.N. Welding Research Supplement, Oct. 50, 1971, pp.434s-440s.
21. Ashby, M.F. and Embury, J.D. Scripta Metallurgica, 19, pp.557-562, 1985.
22. Pollard, B. Metals Technology, 1, 1974, pp.31-36.
23. Semchyshen, M., Bond, A.P. and Durdas, H.J. In Conference Proceedings. Toward improved ductility and toughness, Kyoto, Japan, 1971, pp.239-253.
24. Demo, J.J. Met. Trans., 5, Nov. 1974, pp.2253-2256.
25. Demo, J.J. Ductile chromium- containing ferritic alloys. Canadian Patent No.952741, 13 Aug., 1974.
26. Wright, R.N. Toughness of ferritic stainless steels. ASTM STP 706, R.A. Lula, Ed., ASTM, 1980, pp.2-33.
27. Grubb, J.F., Wright, R.M. and Farrar, P. Micromechanics of brittle fracture in titanium stabilized and alpha'-embrittled ferritic stainless steels. From: Toughness of Ferritic Stainless Steels, ASTM STP 706, R.A. Lula, ed. ASTM, 1980, pp.56-76.
28. Grubb, J.F. Ph.D. thesis, 1982, Rensselaer. Polytechnic Institute.
29. Wood, J.R. Toughness of ferritic stainless steels. ASTM STP 706, R.A. Lula, Ed., ASTM, 1980, pp.145-160.
30. Sipos, D.J., Steigerwald, R.F. and Whitcomb, N.E. U.S. Patent No. 3,672,876, 27 June, 1972.
31. Redmond, J.D. Toughness of ferritic stainless steels, ASTM ST 706, R.A. Lula, Ed., ASTM, 1980, pp.123-144.
32. Demo, J.J. Corrosion, 27, No.12, Dec. 1971, pp.531-544.
33. Lenova, A.N. and Frantov I.I. Welding Production, 11, part 1, 1979, pp.23-26.
34. Goldsteyn, Ya. E., Piskunova, A.I., Shmatko, M.N. and Atapina, G.G. High-temperature brittleness of a ferritic chromium steel, Russ. Metall., (4), 1983, pp.91-94.
35. Demo, J.J. Structure, constitution and general characteristics of wrought ferritic stainless steels, ASTM STP 619, American Society for Testing and Materials, 1977.
36. Williams, R.O. Transacti., Metallurgical Society of the American Inst. of Mining, Metallurgical and Petroleum Engineers, No.212, 1958, pp.497-502.

37. Williams, R.O. and Paxton, H.W. J. Iron Steel Inst., No.185, 1957, pp.358-374.
38. Fisher, R.M., Dulis, E.J. and Carroll, K.G. Trans. AIME, 197, 1953, pp.690-695.
39. Nichol, T.J., Datta, A. and Aggen, G. Met. Trans. A, 11A, April 1980, pp.573-585.
40. DeNeys, T. and Gielen, P.M. Met. Trans., 2, 1971, pp.1423-1428.
41. Grobner, P.J. Met. Trans., 4, 1973, pp.251-260.
42. Yasunaka, T. and Kanao, M. Trans. ISIJ, 19, 1978, pp.57-75.
43. Barrett, C.S. and Massalski. Structure of Metals New York, McGraw-Hill, 1966.
44. Bain, E.G. and Griffiths, W.E. Transactions of the American Institute of Mining and Metallurgical Engineers, 72, pp.166-213.
45. Redmond, J.D. et al. J of Metals, 33, No.2 1981, p.19.
46. Geach, G.A. and Hughes, J.E. The alloys of rhenium with molybdenum or with tungsten and having good high temperature properties. In: F. Benesovsky (ed.), Plasma Proc. 1985, Pergamon Press, Oxford, 1956, pp.245-253.
47. Klopp, W.D., Holden, F.C. and Jaffee, R.I. Further studies on rhenium alloying effects in molybdenum, tungsten, and chromium. Battelle Mem. Ins., 12th July, 1960.
48. Maykuth, D.J. and Gilbert, A. Chromium and chromium alloys. DMIC Report 234, 1 Oct. 1966, Battelle Mem. Inst.
49. Stephens, J.R. and Klopp, W.D. Enhanced ductility in binary chromium alloys. Trans. Metall. Soc., AIME, 242, 1968, pp.1837-1843.
50. Klopp, W.D. Review of Chromium, Molybdenum, and Tungsten Alloys, J. Less Common Metals, 42, 1975, pp.261-278.
51. Edwards, B.C., Eyre, B.L. and Gage, G. Scripta Metallurgica, 28, pp.335-356.
52. Higginson, A. The effect of the addition of ruthenium or palladium on the corrosion resistance of Fe-40Cr, Council for Mineral Technology, Technical Memorandum 19016, 26th July, 1984.
53. Deverell, H.E., McCunn, T.H. and Allegheny Ludlum. U.S. Patent, No. US4456483, 26th June, 1984.



Author Demarsh Elizabeth Anne

Name of thesis A Study Of The Embrittlement And Toughening Of Fe-40% Cr Alloys. 1986

PUBLISHER:

University of the Witwatersrand, Johannesburg

©2013

LEGAL NOTICES:

Copyright Notice: All materials on the University of the Witwatersrand, Johannesburg Library website are protected by South African copyright law and may not be distributed, transmitted, displayed, or otherwise published in any format, without the prior written permission of the copyright owner.

Disclaimer and Terms of Use: Provided that you maintain all copyright and other notices contained therein, you may download material (one machine readable copy and one print copy per page) for your personal and/or educational non-commercial use only.

The University of the Witwatersrand, Johannesburg, is not responsible for any errors or omissions and excludes any and all liability for any errors in or omissions from the information on the Library website.